UNIVERSIDAD NACIONAL DE COLOMBIA

Ph.D. THESIS.

DESIGN AND ANALYSIS OF A MULTI-STAGE CONTROL FOR POWER MULTI-CONVERTERS IN A DC MICROGRID

Author:
MIGUEL EDUARDO MONSALVE RUEDA

Advisor:
FREDY EDIMER HOYOS VELASCO Ph.D.

Co -Advisor:
JOHN EDWIN CANDELO BECERRA Ph.D.

2023

UNIVERSIDAD NACIONAL DE COLOMBIA

Facultad de Minas

Doctorado en Ingeniería – Sistemas Energéticos.

DESIGN AND ANALYSIS OF A MULTI-STAGE CONTROL FOR POWER MULTI-CONVERTERS IN A DC MICROGRID

A DISSERTATION SUBMITTED TO THE DEPARTMENT OF PROCESS AND ENERGY
OF UNIVERSIDAD NACIONAL DE COLOMBIA
IN PARTIAL FULFILLMENT OF THE REQUIREMENTS
FOR THE DEGREE OF
DOCTOR ON ENGINEERING - ENERGY SYSTEMS

Advisor:
FREDY EDIMER HOYOS VELASCO Ph.D.

Co -Advisor:
JOHN EDWIN CANDELO BECERRA Ph.D.

MEDELLÍN - COLOMBIA

2023

TITLE: DESIGN AND ANALYSIS OF A MULTI-STAGE CONTROL FOR POWER MULTI-CONVERTERS IN A DC MICROGRID

ABSTRACT: *MICROGRIDS ARE DESIGNED TO CONNECT DIFFERENT TYPES OF AC AND DC LOADS, WHICH REQUIRE ROBUST POWER CONTROLLERS TO ACHIEVE EFFICIENT ENERGY TRANSFER. HOWEVER, THE EFFECTS OF AC AND DC DISTURBANCES ON A SINGLE TYPE OF CONTROLLER MAKE ACHIEVING SUCH STABILITY IN A MICROGRID A DESIGN CHALLENGE. ADDITIONALLY, IN MULTISTAGE SYSTEMS AND LOADS WHERE DISTURBANCES AFFECT BOTH UPSTREAM AND DOWNSTREAM OF THE MICROGRID, THESE CONTROLLERS DEMAND GREATER ROBUSTNESS. THIS THESIS PRESENTS AN ANALYSIS OF A SLIDING MODE CONTROL (SMC) APPLIED TO A MULTISTAGE MICROGRID WITH DIRECT CURRENT (DC) AND ALTERNATING CURRENT (AC) POWER CONVERTERS. THE GOAL WAS TO IMPLEMENT SLIDING MODE CONTROLLERS FOR CONVERTERS THAT SUPPLY CONSTANT POWER LOADS DC-DC AND DC-AC. THE CONTROLLER WAS TESTED CONSIDERING A UNIQUE SLIDING SURFACE FACING EXTERNAL DISTURBANCES, SUCH AS VARIATIONS IN THE FREQUENCY OF AC CONVERTERS, SUDDEN CHANGES IN UPSTREAM VOLTAGES, AND CONSTANT POWER LOADS (CPL). INITIALLY, THE SIMPLE FIRST-ORDER CONTROLLER WAS ANALYZED, THEN WITH A WASHOUT FILTER, AND SUBSEQUENTLY EXPERIMENTALLY VALIDATED. NEXT, A SECOND-ORDER CONTROLLER WAS ANALYZED. THE INFLUENCE ON THE RESPONSE AND STABILITY OF THE GAIN VALUES (K) OF THE CONTROLLER'S SLIDING SURFACE WAS ALSO STUDIED. THE RESULTS SHOW THAT THE CONTROLLER IS ROBUST IN TERMS OF SENSITIVITY TO EXTERNAL DISTURBANCES AND STEADY-STATE ERROR. HOWEVER, IT WAS OBSERVED THAT THERE ARE LIMITING VALUES FOR THE SLIDING SURFACE CONSTANT 'K,' WHERE IF 'K' IS TOO LOW, DECELERATION OCCURS, AND THE RESPONSE TO DISTURBANCES IS CRITICAL, AND IF IT IS TOO HIGH, UNDESIRED OVERSHOOT OCCURS IN THE OUTPUT VOLTAGE. THIS WAY, IT WAS OBSERVED THAT IT IS POSSIBLE TO FIND A SINGLE CONTROLLER THAT OFFERS SOME ROBUSTNESS TO TYPICAL DISTURBANCES IN A MICROGRID WITH COMMERCIAL VOLTAGES.*

KEYWORDS: *SLIDING MODE CONTROL, MICROGRID, BUCK CONVERTER, HIGHER ORDER CONTROL.*

TÍTULO: DISEÑO Y ANÁLISIS DE UN CONTROL MULTIETAPA PARA MULTICONVERTIDORES DE POTENCIA EN UNA MICRORRED DC

RESUMEN: *LAS MICRORREDES ESTÁN DISEÑADAS PARA CONECTAR DIFERENTES TIPOS DE CARGAS DE CA Y CC QUE REQUIEREN CONTROLADORES DE POTENCIA ROBUSTOS PARA LOGRAR UNA TRANSFERENCIA DE ENERGÍA EFICIENTE. SIN EMBARGO, LOS EFECTOS DE LAS PERTURBACIONES DE CA Y CC EN UN ÚNICO TIPO DE CONTROLADOR HACEN QUE LOGRAR DICHA ESTABILIDAD EN UNA MICRORED SEA UN DESAFÍO DE DISEÑO. ADICIONALMENTE, EN SISTEMAS DE MÚLTIPLES ETAPAS Y CARGAS DONDE LAS PERTURBACIONES AFECTAN TANTO AGUAS ARRIBA COMO AGUAS ABAJO DE LA MICRORED ESTOS CONTROLADORES EXIGEN MAYOR ROBUSTEZ. ESTA TESIS PRESENTA UN ANÁLISIS DE UN CONTROL DE MODO DESLIZANTE (SMC) APLICADO A UNA MICRORRED DE MÚLTIPLES ETAPAS CON CONVERTIDORES DE POTENCIA DE CORRIENTE CONTINUA (DC) Y CORRIENTE ALTERNA (AC). EL OBJETIVO FUE IMPLEMENTAR CONTROLADORES DE MODO DESLIZANTE A CONVERTIDORES QUE ALIMENTAN CARGAS DE POTENCIA CONSTANTES CC-CC Y CC-CA. EL CONTROLADOR FUE PROBADO CONSIDERANDO UNA SUPERFICIE DESLIZANTE ÚNICA QUE ENFRENTA PERTURBACIONES EXTERNAS, COMO VARIACIONES EN LA FRECUENCIA DE LOS CONVERTIDORES DE CA, CAMBIOS REPENTINOS EN LOS VOLTAJES AGUAS ARRIBA Y CARGAS DE POTENCIA CONSTANTE (CPL). INICIALMENTE SE ANALIZÓ EL CONTROLADOR DE PRIMER ORDEN SENCILLO, LUEGO CON FILTRO WASHOUT Y POSTERIORMENTE SE VALIDÓ EXPERIMENTALMENTE. LUEGO SE ANALIZÓ UN CONTROLADOR DE SEGUNDO ORDEN. TAMBIÉN SE ANALIZÓ LA INFLUENCIA EN LA RESPUESTA Y ESTABILIDAD DE LOS VALORES DE GANANCIA (K) DE LA SUPERFICIE DE DESLIZAMIENTO DEL CONTROLADOR. LOS RESULTADOS MUESTRAN QUE EL CONTROLADOR ES ROBUSTO EN CUANTO A SENSIBILIDAD A PERTURBACIONES EXTERNAS Y ERROR DE ESTADO ESTACIONARIO. SIN EMBARGO, SE OBSERVÓ QUE EXISTEN VALORES DE CONSTANTES DE SUPERFICIE DE DESLIZAMIENTO "K" LÍMITES DONDE SI "K" ES DEMASIADO BAJO SE PRESENTA UNA DESACELERACIÓN Y LA RESPUESTA ANTE PERTURBACIONES ES CRÍTICA, Y SI ES DEMASIADO ALTO*

SE PRESENTA UN SOBREPASO INDESEADO EN EL VOLTAJE DE SALIDA. DE ESTA MANERA SE OBSERVÓ QUE ES POSIBLE ENCONTRAR UN ÚNICO CONTROLADOR QUE OFRECIERA CIERTA ROBUSTEZ A LAS PERTURBACIONES TÍPICAS DE UNA MICRORRED CON VOLTAJES COMERCIALES.

PALABRAS CLAVE: *CONTROL DESLIZANTE, MICRORED, CONVERTIDOR BUCK, CONTROL DE ALTO ORDEN, CARGAS DE POTENCIA CONSTANTE.*

Acknowledgements.

To my family, friends, and professors.

To my wife Andrea and my mother Odilia for their unconditional support.

To Miguel Angel for his smile.

To my brothers Orlando and Edwin Arturo for inspiring me every day.

To professors Candelo, Hoyos and Don McKenzie for his assistance in all the critical moments.

CONTENTS

LIST OF FIGURES.

LIST OF TABLES.

1. INTRODUCTION.

This thesis is about control theory applied to microgrids: it is an approach of sliding mode control applied to Buck converters. More specifically, it seeks to address the power converters from a controller design point of view to increase the understanding of the first and second order Sliding Mode Control (SMC). The study object will be a microgrid which contains several Buck converters in different modes as DC-DC, DC-AC, that can be typical in home, or industrial applications.

When controlling microgrids implies switching devices is natural to consider strategies such as variable structure systems. Although it does not seem so common, the control actions with discontinuities are still valid in current research. And Sliding Control, although they have been around for more than two decades, still attracts some interest in today's academia. The purpose of this research is to delve into the study of this type of control applied to a typical microgrid. This microgrid could be of a residential type or of a small industry. Microgrids with various stages of converters have traditionally been controlled with PWM. We want to explore, then, the idea of making this control through a variable structure control such as the Sliding Mode Control. Throughout this investigation, the strengths of this type of control will be exposed as well as its weak points and the opportunities to continue investigating in this field, although as mentioned before, it is a mature development.

The document is divided into 6 chapters. Chapter 2 exposes the sliding Mode control from basic principles, passing with pros and cons and developing some

insights about his mathematical background. Chapter 3 explains the effects of a particular first order Sliding Mode Control with D.C Buck Converter and Chapter 4 develops the same notion from an experimental perspective. In Chapter 5 it is analyzed a set of converters: DC-DC and DC-AC Converters as part of a microgrid. Finally, Chapter 6 summarizes the general conclusions.

1.1 Microgrids

Microgrids can be classified according to various criteria: in terms of demand, capacity of the system and the type of circuits. The topologies can be in terms of power supply or Configuration (see fig. 1.1). The topology of a Microgrid is selected according to control mechanisms of resources, voltage and frequency regulation, transition between operation modes (i.e., island mode to on-grid mode), economic dispatch, renewable sources availability among others [1].

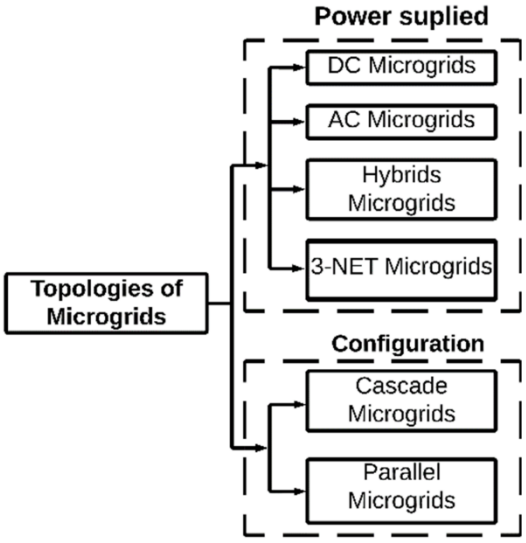

Figure 1.1. *Topologies of Microgrids according from* [1]

The topology of centralized inverter in a DC Microgrid has the advantages of reliability, easy implementation, and low cost. The low cost of this configuration is

due to wiring is relatively simple. Considering a home or small industry application this study considers analysis from power supplied topology: DC and AC microgrids as developed in chapter 4. The idea of the topologies analyzed was that a DC Bus from starting point of connection to various types of loads: DC and AC. The disturbances in this topology were considered upstream oscillations mainly.

1.2 Buck Converter.

Buck converter is a power converter that aims to keep voltage in a set reference (lower than the input) and is categorized as a switched-mode power supply. It contains the elements: diode, an active switch (usually a MOSFET semiconductor), capacitor and one inductor (see topology in figure 1.2). The Buck converter requires a switching element that operates in two modes depending on the current on the inductor IL: continuous conduction mode (CCM) or discontinuous conduction mode (DCM). When the current cross the zero value then the switch works on DCM and when the current has higher values or never cross zero it works on CCM. When the converter operates in the CCM and in steady-state stability, then the voltage output can be expressed by the following equation:

$$D = \frac{< V_o >}{V_i} \quad (1)$$

Where D refers to the Duty cycle, Vo is the average voltage output and Vi is the DC voltage input.

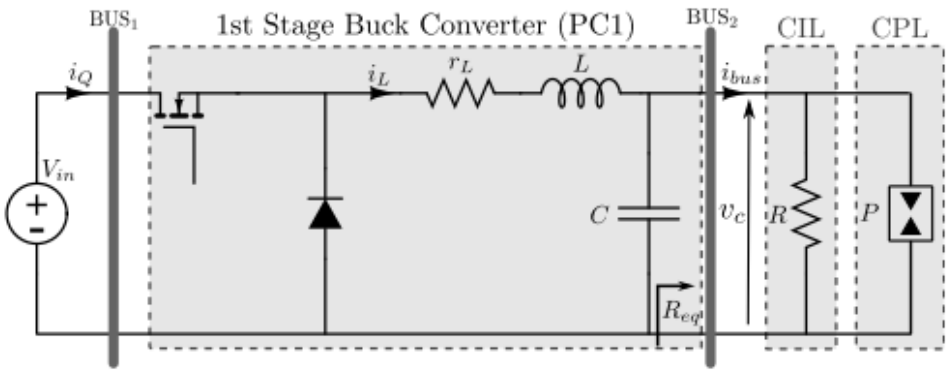

Figure 1.2. *Buck converter with CIL and CPL. Source:* [2].

However, when feeding Constant Power Loads (CPL) by a Buck converter, the results shows that the open loop control is unstable in CCM. So, the system will have additional restrictions on the control in comparison with a purely resistive load [3]. Many techniques have been developed to compensate the system: Damping, Small Signal Analysis, Lyapunov stability, linearized feedback, Droop Mode Control, filters, vector control, d-q Frame Analysis and the SMC are some of them. Those techniques can act in different regions of the system: feeder side or intermediate circuits and load side [4]. Acting in the feeder side

The SMC control will be implemented in the research as part of the intermediate circuits. Similarly, Alternating Current Constant Power Loads (AC-CPL) modeling is still challenging in microgrids [5]. This type of loads also will be considered as part of the present research analysis.

Hence the control of the active switch is fundamental in the operation of the converter. So, for switching control purposes the SMC has been recurrently used in Buck converter topologies [2,6,7]. Sliding control modes have been studied extensively during the 1970s and their great use is mainly due to their advantages

over parameter variations and their tolerance to disturbances [8]. Sliding mode control is a specific type of variable structure control (VC) and it has been successfully utilized in many applications such as electric motors, chemical processes, power systems and robots. VC algorithm is based on the change of its control law depending on the state or performance of the system, and for this reason it is called a control of variable structure. Particularly, the SMC (as mentioned is a VC type control) is designed to drive and then constrain the system state to lie within a neighborhood of the switching function. However due to the negative impedance of the CPL load and the uncertain points of equilibrium that produce is required a different control beyond purely linearize the signal. Traditional techniques have been developed to control CPLs like Proportional-Integral (PI) algorithms[9] and another different technique used is the washout filter. The idea within the washout filter is that filtering the signal to explicitly derive a control law allows to automatically reach the equilibrium [6]. Therefore, to implement a washout filter ensures some robustness under variations in the CPL via filtering the inductor current. See example equations 2 and 3 of the SMC control law used in a Buck converter with a washout filter [2].

$$f^{+}(x) = \begin{bmatrix} \dot{\imath L} \\ \dot{V c} \\ \dot{Z} \end{bmatrix} = \begin{bmatrix} \frac{1}{L}(V_{in} - V_c - r_L i_L) \\ \frac{1}{C}\left(i_L - \frac{V_c}{R} - \frac{P}{Vc}\right) \\ w(i_L - Z) \end{bmatrix}, \qquad (2)$$

$$f^{-}(x) = \begin{bmatrix} \dot{\imath L} \\ \dot{V c} \\ \dot{Z} \end{bmatrix} = \begin{bmatrix} \frac{1}{L}(-V_c - r_L i_L) \\ \frac{1}{C}\left(i_L - \frac{V_c}{R} - \frac{P}{Vc}\right) \\ w(i_L - Z) \end{bmatrix}, \qquad (3)$$

Even though, to complete the analysis in the microgrid the main DC Bus requires a control that allows the system stability due to disturbances in the system, i.e., absence of the main grid[10]. Many strategies and control techniques can be

developed for this purpose. Controls as PID, Fuzzy, Predictive, or even SMC as well have been analyzed in the literature of each of the next chapters.

1.3 Variable Structure Systems (VSS).

The idea behind of variable structure systems is to change the structure of the control law with the idea of achieving the control objectives in finite time [11]. These systems are widely used in processes that require high maneuverability and systems which need to be highly responsive and highly energy efficient. Similarly, to classic control, in Variable Structure Systems full-state feedback is used. However, considering that eigenvalues do not apply to study stability in non-linear systems have been proposed other techniques as H-infinity, Hyperstability and Lyapunov. In the present study, only the theory concerning Lyapunov stability will be developed. The following example illustrates the theory behind Lyapunov stability:

$$\dot{X} = AX + BU \tag{1}$$

$$\sigma = CX \tag{2}$$

$$V = \frac{1}{2}\sigma^{\tau}\sigma > 0 \tag{3}$$

$$\dot{V} = \sigma^{\tau}\dot{\sigma} < 0 \tag{4}$$

Then,

$$(CV)^{T}\left(C\dot{X}\right) \tag{5}$$

$$X^{\tau}C^{\tau}|(CAX + CBU) < 0 \tag{6}$$

If,

$$|CBU| > |CAX| \tag{7}$$

$$CB > 0$$

Then,

$$X^{\tau}C^{\tau}|(CBU) < 0 \quad (8)$$

$$X^{\tau}C^{\tau}U < 0 \quad (9)$$

Let,

$$U = -\alpha.sign(x) \quad (10)$$

Where,

$$|CB\alpha| > |CAx| \quad (11)$$

2. SLIDING MODE CONTROL.

Despite the evolution of other types of control like robust adaptive control, the sliding mode control is still an effective choice to deal uncertainties and disturbances. The Sliding Mode Control (SMC) is a time domain particular control of Variable Structure Systems (VSS) where results are obtained after a variation between structures in real time. Then, the design problem is to select the parameters of each of the structures and to define the switching logic [11]. Classical example by professor Utkin examines the control based in achieving asymptotic stability switching between two structures:

$$[\Psi] = \begin{bmatrix} \alpha_1, & if\ x\dot{x} > 0 \\ \alpha_2, & if\ x\dot{x} > 0 \end{bmatrix}$$

As a result, there is obtain the phase plane shown below:

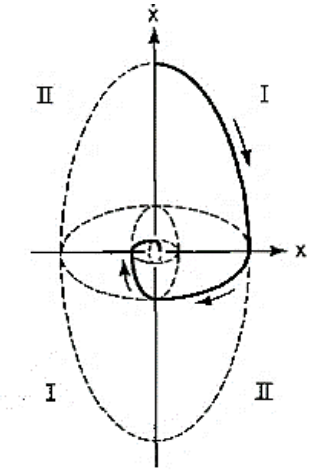

Figure 2.1. *Phase portrait by Utkin in* [11].

The idea resulting from applying this change in structure is that the control becomes more robust against disturbances and rejects them almost completely. Ideally, in this phase plane the trajectories will converge to the origin, where the variable controlled is stable. The robustness of this system will be analyzed in terms of stability, where there is a certain convergence region, which under some disturbances the response will remain inside this region but without adequate control it will not converge to the origin. Then, in Sliding Mode Control a sliding surface is defined. In which depending on the dimension of the applied system, it will be a line, or a hyperplane. Ideally, the trajectories in my system will reach this hyperplane as soon as possible looking the best energy efficiency of the control. With the idea of calculating this distance it will be defined a parameter sigma, and his first derivative giving some speed.

2.1 Mathematical description.

We define a region Ω (*K1, K2, L*) in the phase plane:

x2

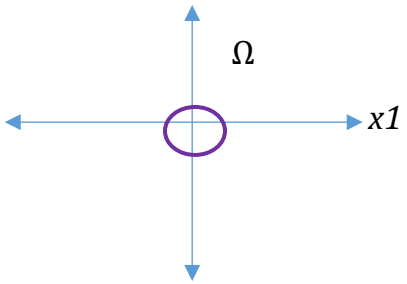

With a hyperplane, or sliding surface:

$$\sigma = \sigma(x_1, x_2) = x_2 + cx_1 \ , \qquad c > 0$$

Whose first derivate is:

$$\dot{\sigma} = cx_2 + f(x_1, x_2, t) + u \ , \qquad \sigma_0 = \sigma(0)$$

For instance, the origin of this hyperplane is an equilibrium point. Then, the control objective will be that the distance of each trajectory point to this hyperplane is close to zero.

We introduce a Lyapunov function:

$$V = \frac{1}{2}\sigma^2$$

$$\dot{V} < 0 \ for \ \sigma \neq 0$$

$$\dot{V} = \sigma\dot{\sigma} = \sigma(cx_2 + f(x_1, x_2, t) + u)$$

$$u = -cx_2 + v$$

$$\dot{V} = \sigma\dot{\sigma} = \sigma(cx_2 + f((x_1, x_2, t) + \sigma v \leq |\sigma|L + \sigma v$$

If the origin is a global and asymptotically stable point. Even though this point will converge in a finite time. That is one of the most prevailing characteristics of sliding mode control.

$$v = -\rho sign(\sigma)$$

$$,\rho > 0$$

$$sign\,(x) = \begin{Bmatrix} 1\,, & if\ x > 0 \\ -1, & if\ x < 0 \end{Bmatrix}$$

The convergence time is given by:

$$T(\sigma_0) \leq\ -\alpha V^{1/2}$$

Finally, our control will be:

$$u = -cx_2 - \rho sign(\sigma)$$

This control signal has two components: a continuous element and a discontinuous given by sign(σ). This discontinuous component has the property of force the system asymptotically to the origin, thus corresponding to the control objective.

2.2 Chattering in power systems.

Chattering avoidance is one of the most important considerations when designing a Sliding Mode Control. Due to his own nature and discontinuous operation, SMC can produce a chattering response, which is undesirable in some applications as motors, airflights actuators and power systems. The obvious solution to make the control function $-\rho sign(\delta)$ is to approximate the discontinuous function by other continuous with similar properties as a “sigmoid function” [12]. The slope of this transition given by this function will be produced by the factor "a" in this function and can be the subject of analysis within the answers to be obtained (fig. 2.2).

$$sign(\sigma) \approx \frac{\sigma}{|\sigma| + \varepsilon}$$

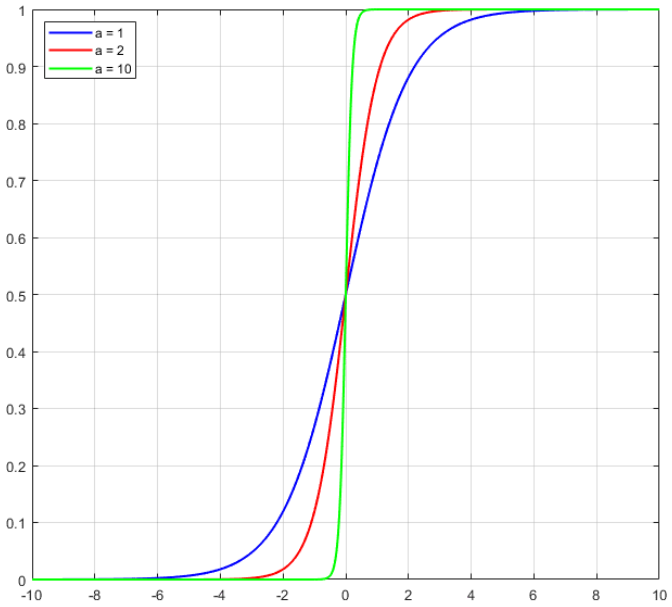

Figure 2.2. *Sigmoid plots for three "a" factor (own elaboration).*

When it is replaced the original sign function with this "sigmoid" function into the control, then implicitly it is replaced de discontinuous function by other continuous function with a quasi-similar behavior and this is also called quasi-sliding mode control.

2.3 Higher Order Sliding Mode Control

As an example for higher order is showed in figure 2.3 the typical phase diagram is presented for the author Shteseel [12]:

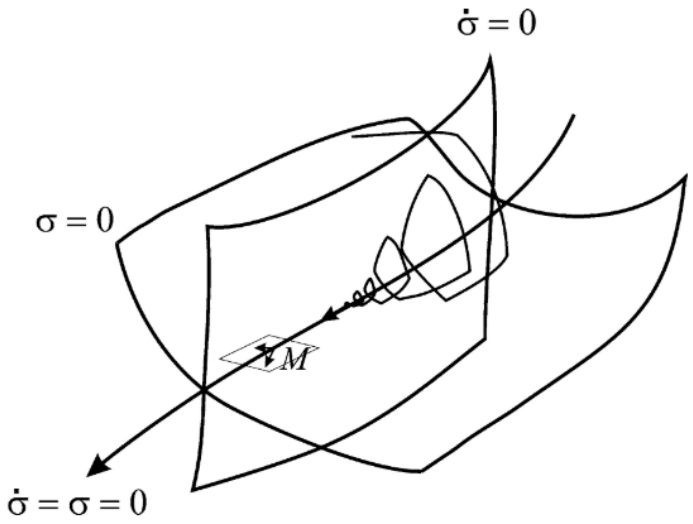

Figure 2.3. *Second Order sliding Mode Control Vectors* [12].

This type of controller will be implemented and described in Chapter 5. In this chapter a single controller will be tested across multiple stages of a microgrid and reviewed.

References

1. Cabana-Jiménez, K.; Candelo-Becerra, J.E.; Sousa Santos, V.; Santos, V.S. Comprehensive Analysis of Microgrids Configurations and Topologies. *Sustainability* **2022**, *14*, 1056, doi:10.3390/su14031056.

2. Tahim, A.P.N.; Pagano, D.J.; Heldwein, M.L.; Ponce, E. Control of Interconnected Power Electronic Converters in Dc Distribution Systems. *COBEP 2011 - 11th Brazilian Power Electronics Conference* **2011**, 269–274, doi:10.1109/COBEP.2011.6085269.

3. Grigore, V.; Hatonen, J.; Kyyra, J.; Suntio, T. Dynamics of a Buck Converter with a Constant Power Load. *PESC Record - IEEE Annual Power Electronics Specialists Conference* **1998**, *1*, 72–78, doi:10.1109/PESC.1998.701881.

4. Hossain, E.; Perez, R.; Nasiri, A.; Padmanaban, S. A Comprehensive Review on Constant Power Loads Compensation Techniques. *IEEE Access* **2018**, *6*, 33285–33305, doi:10.1109/ACCESS.2018.2849065.

5. Dong, Y.; Liu, W.; Gao, Z.; Zhang, X. New Simulation Model of Ac Constant Power Load. *Hangkong Xuebao/Acta Aeronautica et Astronautica Sinica* **2009**, *30*, 115–120, doi:10.1109/TENCON.2008.4766537.

6. Pagano, D.J.; Ponce, E. On the Robustness of the DC-DC Boost Converter under Washout SMC. *2009 Brazilian Power Electronics Conference, COBEP2009* **2009**, 110–115, doi:10.1109/COBEP.2009.5347639.

7. Yue, Z.; Wei, Q. A Third-Order Sliding-Mode Controller for DC/DC Converters with Constant Power Loads. *Conference Record - IAS Annual Meeting (IEEE Industry Applications Society)* **2011**, 1–8, doi:10.1109/IAS.2011.6074347.

8. Bandyopadhyay, B.; Deepak, F.; Kim, K.S. *Sliding Mode Control Using Novel Sliding Surfaces*; 2009; Vol. 392; ISBN 9783642034473.

9. Rivetta, C.H.; Emadi, A.; Williamson, G.A.; Jayabalan, R.; Fahimi, B. Analysis and Control of a Buck DC-DC Converter Operating with Constant Power Load in Sea and Undersea Vehicles. *IEEE Trans Ind Appl* **2006**, *42*, 559–572, doi:10.1109/TIA.2005.863903.

10. Kakigano, H.; Nishino, A.; Miura, Y.; Ise, T. Distribution Voltage Control for DC Microgrid by Converters of Energy Storages Considering the Stored Energy. *2010 IEEE Energy Conversion Congress and Exposition, ECCE 2010 - Proceedings* **2010**, 2851–2856, doi:10.1109/ECCE.2010.5618178.

11. Utkin, V. Variable Structure Systems with Sliding Modes. *IEEE Trans Automat Contr* **1977**, *AC-22*, 212–222.

12. Shtessel, Y.; Edwards, C.; Fridman, L. *Sliding Mode Control and Observation, Series: Control Engineering*; Birkhauser, 2016; Vol. 10; ISBN 978-0-81764-8923.

3. DYNAMIC BEHAVIOR OF A SLIDING-MODE CONTROL BASED ON A WASHOUT FILTER WITH CONSTANT IMPEDANCE AND NONLINEAR CONSTANT POWER LOADS.

(This article belongs to the Special Issue Simulation-Based Validation and Design of Smart Grids - Appl. Sci. 2019, 9(21), 4548; https://doi.org/10.3390/app9214548).

Abstract

Power converters (PCs) with their control techniques help regulate voltages of nodes in microgrids with different types of loads such as resistive, inductive, nonlinear, constant power, or critical loads. However, constant power loads (CPLs) affect the stability of the voltage in the output of PCs and are usually difficult to regulate with traditional control techniques. The sliding-mode control (SMC) with the washout filter technique has been recently proposed to address this issue, but studies that consider the phenomenon and parameters present in real systems are required. Therefore, this paper focuses on evaluating the dynamic behavior of an SMC based on a washout filter using three different loads: A constant impedance load (CIL), a nonlinear CPL, and a combination of CIL and CPL. The CIL considered a resistance connected to the circuit, whereas the nonlinear CPL was designed by using a buck converter with zero average dynamics and fixed-point induction control techniques (ZAD-FPIC). The tests consisted of creating some variations in the reference signals to identify the output voltage and the error that the control brings according to the different loads. Besides, this study focuses on representing the dynamic behavior of signals when loads change, considering quantization effects, system discretization, delay effects, and parasitic resistors. Additionally, bifurcation diagrams are created by changing the control parameter k and plotting the regulated voltage and the error produced in the output signals. To illustrate the advantages of the SMC with the washout filter technique, a comparison was made with other techniques such as the proportional–integral–derivative (PID) and conventional SMC by varying the load. The results showed that SMC with the washout filter technique was superior to the PID and the conventional SMC because it stabilizes the signal faster and has a low steady-state error. Additionally, the control system regulates well the output voltage with the three types of load and the system remains stable when changing the parameter k for values greater than 1, with a low error in the steady-state operation.

Keywords: *DC-DC power converters; constant impedance load; constant power load; sliding-mode control; washout filter; ZAD-FPIC.*

3.1 Introduction.

Renewable energy is an important source in microgrids (MGs) [1, 2], as it can help provide power to end users [3]. Power converters (PCs) are used to transfer power from these sources to users and help regulate voltage and improve energy efficiency [2, 4]. The use of PCs in MGs has increased in recent years [5] and some electronic devices are now used to transfer power from alternating to direct current (AC-DC), and from direct-to-direct current (DC-DC) [6,7], forming different voltage levels in the network that must be controlled. Although, many stability problems have been studied in AC systems, the PCs can create unstable events in DC systems when the load changes [7]. Thus, this dynamic behavior is of great importance as the development of MGs continues, and better analysis must be performed.

Sliding-mode control (SMC) is a specific type of variable structure control (VSC), which was studied extensively during the 1970s. Its widespread use is mainly due to its advantages over parameter variations and tolerance to disturbances [8]. The main feature of VSC is sliding motion, which is when the system state repeatedly crosses certain subspaces or sliding hyperplanes [9]. Moreover, washout filters are extensively used to control chaotic systems and have recently been used in PCs in conjunction with SMC controllers [10]. Some authors have proposed the use of SMC with washout filters [11, 12] as a good option to control the output voltage regarding load variations. The idea when implementing a washout filter in a PC is to ensure some robustness under variations in the constant power load (CPL) via filtering the inductor current.

Particularly in [11], nonlinear stability analysis of a standalone DC network and an SMC based on a washout filter is used to maintain constant DC bus voltage. In this case, the authors show the behavior of the system with the controller under nonlinear load variations. Besides, in [12], an SMC with a washout filter is used to regulate the

DC bus voltage under constant impedance load (CIL) and constant power load (CPL). They also determined the operating limits of the controlled system in terms of the maximum power drained by the CPL and CIL connected to the bus. In [13], the authors study stability issues in DC MGs with instantaneous CPL, as this load introduces a destabilizing effect in DC MGs that brings significant oscillations of the voltages or reaches system collapse. Some strategies, such as load shedding, addition of resistive loads, filters or energy storage directly connected to the main bus, and control methods, are applied.

Commonly, studies do not compare the control performance to different types of loads and, especially, nonlinear CPLs. CPL loads have the characteristic of negative incremental impedance, which may cause system instability during disturbances if the system is not properly controlled [14]. Hence, when feeding a CPL by a buck converter, the results show that the open-loop control is unstable in continuous conduction mode (CCM). Therefore, the system will have additional restrictions on the control in comparison to a purely resistive load [15]. Many techniques have been developed to compensate the system, e.g., damping, small-signal analysis, Lyapunov stability, linearized feedback, droop mode control, filters, vector control, d–q frame analysis, and SMC. However, the authors of [16] reveal that there are three stabilization techniques used to compensate the negative impedance of CPL: the Feeder side, intermediate circuits, and load side. On the other hand, the authors of [17] classify the compensation techniques into passive and active damping, space pole placement control, pulse adjustment control, SMC, model predictive control, and feedback linearization.

Papers found in the literature show that few studies consider phenomena and parameters present in real systems and do not consider bifurcation diagrams to evaluate the performance of the buck converter. Therefore, this paper focuses on studying the dynamic behavior of an SMC based on a washout filter to control the voltage when the load is formed by a combination of CIL and CPL. The voltage

reference signal was changed to evaluate the response of the controller to different types of load. To perform the test, an electronic circuit was modeled and simulated that considers internal resistances, system discretization, quantization effects, and delay effects in order to study a more realistic circuit as in [18, 19]. Finally, a numerical bifurcation was performed by changing the parameters k with the aim of visualizing the nonlinear effects of the circuit and the load. All these tests were validated by measuring the voltage in the output bus (υc).

Contributions of this paper with respect to the literature are as follows: 1) The dynamic behavior of the SMC is evaluated with different types of load; 2) quantization, system discretization, parasitic resistors, and delay effects are modeled to obtain closer results to real circuits; 3) a buck converter with a quasi-sliding control technique is used as a CPL load, which converts it to a nonlinear CPL; 4) unstable zones and steady-state errors are obtained to evaluate the system stability when the control parameters are changed; 5) bifurcation diagrams for the output voltage and voltage error are used to evaluate the response of the controller in the steady-state operation under changes in the control parameter k; and 6) comparisons among the proportional–integral–derivative (PID), conventional SMC, and SMC with a washout filter are performed with variations in CIL and CPL. Therefore, the materials and methods used in this research along with the mathematical fundamentals, simulations, and simulated electronic circuit are presented in Section 2. The results, analysis, and discussion are included in Section 3, and Section 4 presents the conclusions.

3.2 Materials and Methods.

Next, the mathematical models of the network elements and power controller are presented. Thus, the SMC that considers the washout filter is included with the

detailed information needed to study the effects on the controller. Besides, an electronic circuit is modeled to simulate the effects of load changes and evaluate the effects created in the network with voltage reference variations. Finally, bifurcation diagrams are plotted to evaluate the stability of the electric circuit with different loads.

3.2.1. Microgrid.

AC-DC and DC-DC PCs are used to transfer power to the different loads in the MG [12], as shown in Figure 3.1. DC-DC PCs are used to connect sources, such as photovoltaic panels and batteries, to the input bus (Bus 1). AC-DC PCs are used to connect wind generators and the power grid to the input bus (Bus 1). Furthermore, a buck converter is used to connect the system to other buses and regulate load nodes such as the DC-DC PC connected between Bus 1 and Bus 2 in Figure 3.1. The last PC is an SMC with a washout filter (identified in Figure 3.1 as PC SMC). The final stage in this circuit considers the loads as a CIL connected directly to the DC voltage and a CPL formed by a PC with zero average dynamics and fixed-point induction control techniques (ZAD-FPIC), identified in Figure 1 as PC ZAD-FPIC.

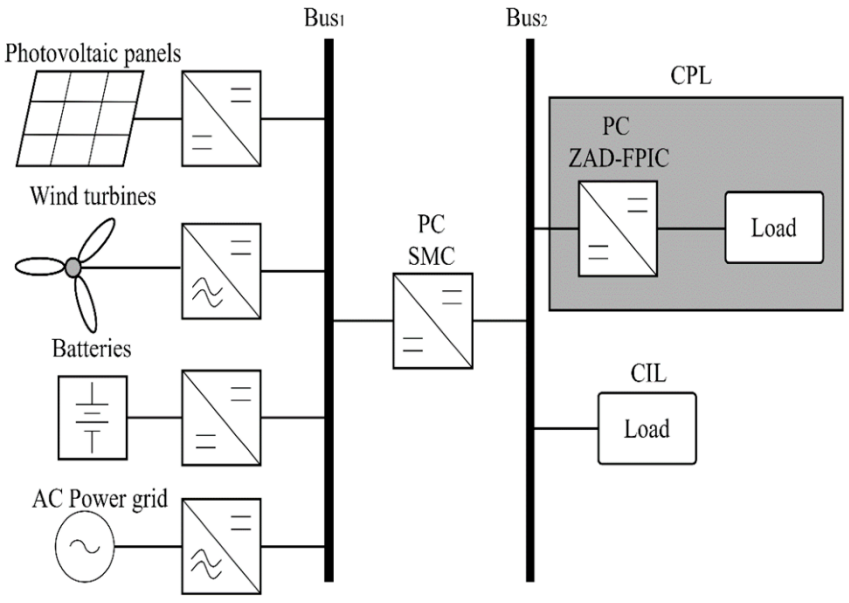

Figure 3.1. *Simplified power network feeding direct current (DC) loads.*

3.2.2. Simplified Model of the Network.

Figure 3.2 shows the DC distribution network implemented to analyze the different effects of the load variation. The converter has a power source with voltage E and an internal source resistor r_s, which represent the equivalent circuit of different energy sources and their internal impedance connected to Bus 1 as shown in Figure 1. A Metal–Oxide–Semiconductor Field-Effect Transistor (MOSFET) working as switch S, an internal MOSFET resistance r_M, a diode D with forward voltage diode V_{fd}, a filter *LC*, an internal resistance of the inductor r_L, and a resistance used to measure current r_{Med}. Finally, Bus2 represents the output of the circuit where the load is connected (CPL and CIL).

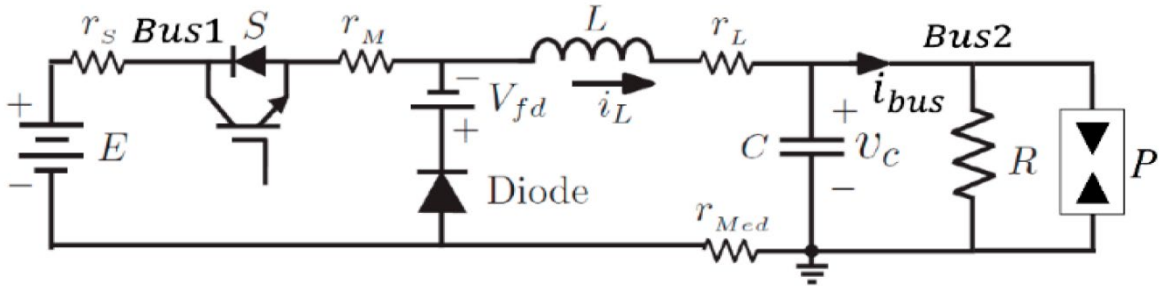

Figure 3.2. *Circuit model of the buck power converter (PC) connected to the constant impedance load (CIL) (R) and constant power loads (CPLs) (P).*

A diagram of the pulse width modulation (PWM) controller connected to the buck converter and the sensors used to measure the different input signals is presented in Figure 3.3. An SMC with a washout filter is used to regulate the output signal. The response to the dynamics created according to the load variation (CPL and CIL) can be regulated by this SMC.

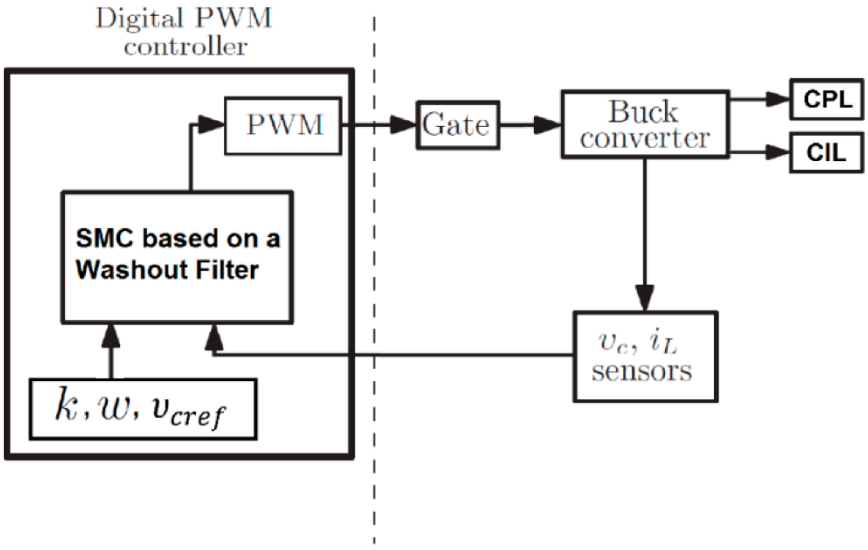

Figure 3.3. *Block diagram of the buck converter with the pulse width modulation (PWM) controller used for the simulation.*

This circuit was used to represent the mathematical and numerical models that are solved to identify the variations and response of the system. Model parameters that help represent the system are discretization, quantization, and delay effects as those obtained for real circuits.

Figure 3.4 shows the complete diagram implemented in MATLAB-Simulink to control the buck converter using the SMC with a washout filter. The quantization effects are included as 12 bits for the voltage in the condenser v_c and the current in the inductor i_L. A delay period was included in the numerical simulation equal to 1/Fc. The zero-order-hold block is necessary to simulate the fixed sample time and obtain v_c and i_L, and calculating u is explained in the following mathematical model. All parameters of the buck converter and the SMC controller are shown in Table 3-1.

Parameter	Description	Value
R	Resistance of the load	20.44 Ω, 40.092 Ω
C	Capacitance	938 µf
L	Inductance	53.35 mH
r_L	Internal resistance of the inductor	1.33 Ω
r_{Med}	Sensor resistance	1.007 Ω
r_M	Internal resistance of the MOSFET	0.3 Ω

r_s	Internal resistance of the source	0.3 Ω
E	Input voltage	40 V (Dual source)
Fc	Commutation frequency	variable

Table 3-1 Parameters of the circuit used in the direct current (DC) test.

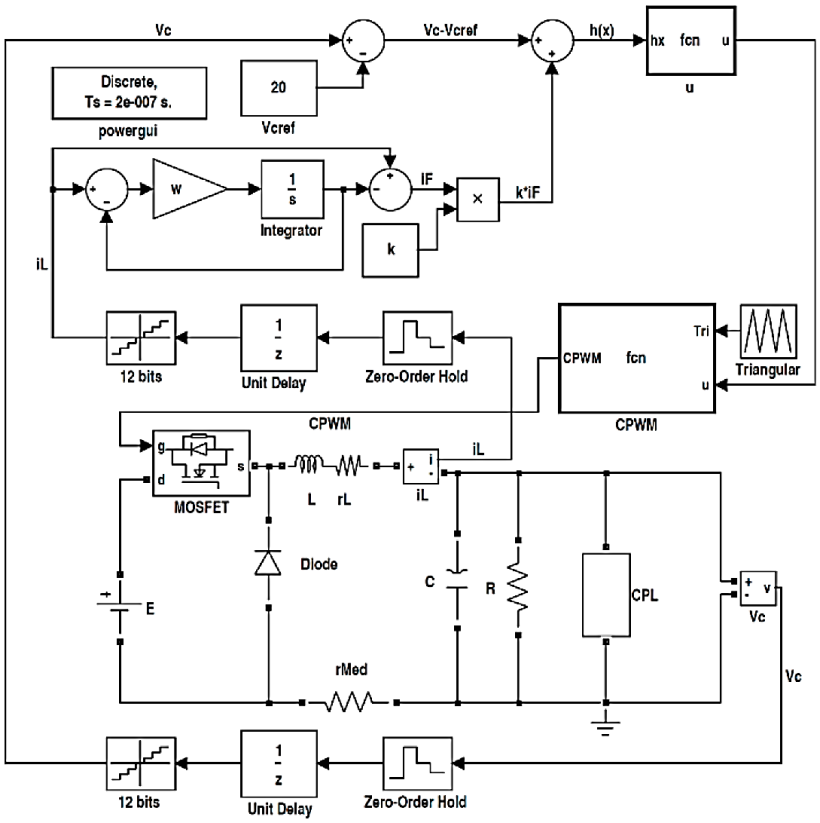

Figure 3.4. *Diagram of the global system for the simulation.*

3.2.3. Mathematical Model of the Controller.

Then, the total current supplied by the electrical circuit is equal to the sum of the current in the CIL and the current in the CPL, as shown in Equation (1):

$$i_{bus} = \frac{v_c}{R} + \frac{P}{v_c}, \tag{1}$$

where i_{bus} is the current supplied by the circuit, R is the constant resistance of the CIL, P is the active power of the CPL, and v_c is the voltage of the capacitor. The equivalent resistance of the circuit can be obtained according to the voltage and the current in the bus as expressed in Equation (2):

$$R_{eq} = \frac{v_c}{i_{bus}}. \quad (2)$$

3.2.4. Dynamics of Buck Converter (PC SMC).

The mathematical models used to represent the dynamics of a buck converter feeding the CIL and CPL are presented in Equations (3) and (4):

$$L\frac{di_L}{dt} = uE - v_c - (r_s + r_M + r_{Med} + r_L)i_L, \quad (3)$$

$$C\frac{dv_c}{dt} = i_L - \frac{v_c}{R} - \frac{P}{v_c}. \quad (4)$$

In these equations, L is the inductor, C is the capacitor, v_c is the instantaneous voltage of the capacitor, and i_L is the instantaneous current of the inductor. As defined previously in the model, the term E is the voltage of the power source, r_s is the internal source resistor, r_M is an internal MOSFET resistance, r_L is an internal resistance of the inductor, and r_{Med} is the resistance used to measure current. The term R represents the constant resistance of the load connected to the bus, P is the active power of the load, and u is used to represent the switching function with values {0,1}.

3.2.5. Voltage Measurement.

The voltage in Bus 2 can be measured and used as an input for the SMC. This can be represented as v_m and is equal to the voltage at Bus 2 and the capacitor voltage:

$$v_m = v_c = V_{Bus2} \quad (5)$$

This value will be changed according to the regulation of the SMC with a washout filter. The final voltage magnitude depends on the voltage reference and the regulation limits allowed in the circuit.

3.2.6. Washout Filter

This method consists of passing the inductor current i_L through a washout filter as shown in Figure 3.4. After the filter, a transfer function is used to obtain the final signal I_F or the filtered inductor current. The transfer function G_F is then used to

obtain a new filtered current as expressed in Equation (6) [2]. Herein, the term s corresponds to the Laplace expression and w is the cut-off frequency of the high-pass filter:

$$G_F(s) = \frac{I_F(s)}{I_L(s)} = \frac{s}{s+w} = 1 - \frac{w}{s+w}. \quad (6)$$

After the induction current is filtered, a differential equation is created and added to the model, as expressed in Equation (7) [11,12], where z is obtained from the integration of Equation (7) [20]:

$$\frac{dz}{dt} = w(i_L - z). \quad (7)$$

3.2.7. Sliding-Mode Control.

The circuit shown in Figure 3.4 has an SMC that receives two signals: v_c that correspond to the capacitor voltage and I_F, which is the filtered inductor control coming from the washout filter. Then, a control law is applied to determine the final output signal, depending on the two switching stages as shown in Equation (8) [2], where u is a scalar that depends on x and can take two values: $u^- = 0$ and $u^+ = 1$. Thus, two conditions are presented depending on the conditions of the output of the function $h(x)$ with $x = \{i_L, v_c, z\}$:

$$u = \begin{cases} u^- = 0, & if \quad h(x) > 0 \\ u^+ = 1, & if \quad h(x) < 0 \end{cases} \quad (8)$$

The system obtains a response of $h(x)$ that is defined in Equation (9) [2]. In this equation, v_c corresponds to the capacitor voltage, v_{cref} is the voltage reference required to regulate the system, i_L is the inductor current, and z is the current difference obtained in the output of the circuit. The term k is a parameter used in the controller that multiplies the filtered current and takes a value greater than zero ($k >$

0). This parameter k can be adjusted in the controller to obtain the different responses of the system and it will be changed to identify the dynamics of the system:

$$h(x) = v_c - v_{cref} + k(i_L - z) = 0. \quad (9)$$

The continuous conduction mode of the system is presented considering Equations (10) and (11). First, when the switch is in the ON state, the resulting equations of the current, voltage, and z are as shown in Equation (10):

$$f^+(x) = \begin{bmatrix} \dot{i}_L \\ \dot{v}_c \\ \dot{z} \end{bmatrix}_{u=1} = \begin{bmatrix} \frac{1}{L}(uE - v_c - (r_s + r_M + r_{Med} + r_L)i_L) \\ \frac{1}{C}\left(i_L - \frac{v_c}{R} - \frac{P}{v_c}\right) \\ w(i_L - z) \end{bmatrix}. \quad (10)$$

When the switch is OFF, a vector field is presented with the new equations of the inductor current, capacitor voltage, and z, as shown in Equation (11):

$$f^-(x) = \begin{bmatrix} \dot{i}_L \\ \dot{v}_c \\ \dot{z} \end{bmatrix}_{u=0} = \begin{bmatrix} \frac{1}{L}\left(-v_c - (r_{Med} + r_L)i_L + v_{fd}\right) \\ \frac{1}{C}\left(i_L - \frac{v_c}{R} - \frac{P}{v_c}\right) \\ w(i_L - z) \end{bmatrix}. \quad (11)$$

3.2.8. Model of the CPL.

The CPL considered is a buck converter as presented in [13], where the final load is a resistance that is controlled by ZAD-FPIC techniques, which are widely used in other research [14]. This technique, proposed in [15], consists of defining a function and forcing an average value of zero at each sampling period [16]. Let us consider $s\big(x(kT)\big)$ as a piecewise linear function of the state value and described by Equation (12) during a complete sampling period:

$$s\big(x(kT)\big) = v_c - v_{cref} + k_s\big(\dot{v}_c - \dot{v}_{cref}\big). \quad (12)$$

The mathematical description for the condition of zero average dynamics is given by (13). The piecewise function $s\big(x(kT)\big)$ is required to obtain information from the state values v_c and i_L at the instant kT

$$\int_{kT}^{(k+1)T} s\big(x(kT)\big)dt = 0. \tag{13}$$

Equation (13) is solved to obtain the duty cycle $d_{k(kT)}$ at each sampling time, which ensures the condition of zero average dynamics when applied to the system through switch S. The duty cycle was obtained in [13,15] with Equation (14) as the buck converter controlled by zero average dynamics (ZAD):

$$d_{k(kT)} = \frac{2s_1(kT) + T\dot{s}_-(kT)}{T(\dot{s}_-(kT) - \dot{s}_+(kT)}. \tag{14}$$

Then, the ZAD-FPIC techniques applied to the buck converter to obtain a new duty cycle are expressed in Equation (15) [24]:

$$d_{ZAD-FPIC}(kT) = \frac{d_k(kT) + Nd^*}{N+1}. \tag{15}$$

Then, the term $d_k(kT)$ is obtained from Equation (14) and d^* can be calculated at the beginning of each period as in Equation (16):

$$d^* = d_k(kT)|_{steady\ state.} \tag{16}$$

3.3. Results.

The following results validate the nonlinear SMC based on a washout filter with the CIL (40 Ω) and CPL (10 W). For the simulation, the voltage reference and the control parameter k are changed to represent variations in the circuit. The results are presented to show the robustness of the control, the voltage regulation, and the transient response of the controller.

3.3.1. Regulation of DC-DC Signals

Comparisons among the circuits working with CIL, CPL, and CIL-CPL are performed, starting with the voltage regulation value $v_{cref} = 32$ DC Volts. The chosen parameters of the LC filter are $L = 53$ mH, $C = 938$ µF, and the switching frequency Fc = 5 kHz, which cause a slower response time of the system; however, it maintains the voltage regulation within the limits with an error close to 3%. Figure 5 shows the behavior of the output voltage v_c and error for the different loads. Figure 5a shows that the voltage follows the reference signal $v_{cref} = 32$ V for the loads and an overshoot of 12.5% is observed for the signal v_c when the load is CPL: 9.5% for CIL and 9% for CIL-CPL. The settling times are similar for the three signals and the steady-state errors are similar and lower than 1.5% as shown in Figure 5b. These curves were created with the factor $k = 4$ and voltage reference $v_{cref} = 32$ V.

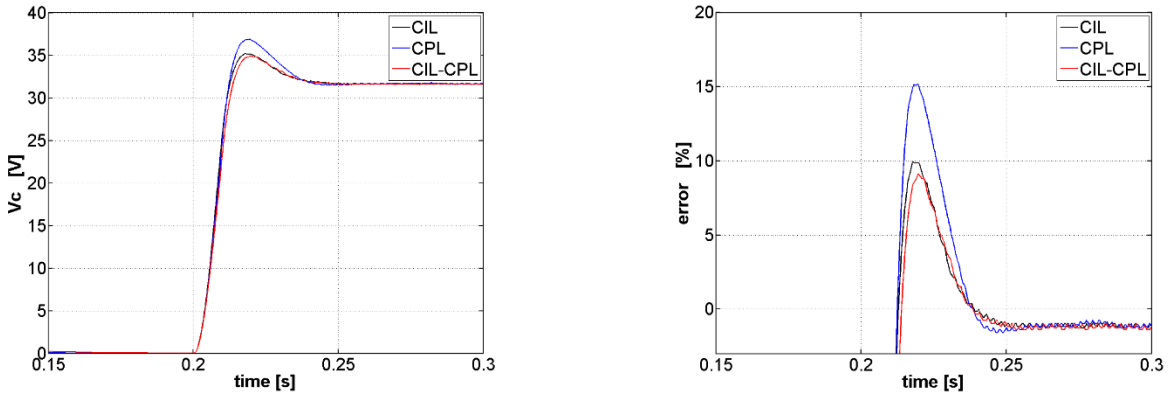

(**a**) output voltage v_c (**b**) error in v_c

Figure 3.5*. Simulated tests with k=4 and voltage regulation of Vcref =32 for loads CIL, CPL, and CIL-CPL.*

Figure 3.6 shows the inductor currents for the three loads and transient behavior. The three currents have similar behavior in the transient and steady-state operations, changing only the final magnitude of the current as they vary according to the load.

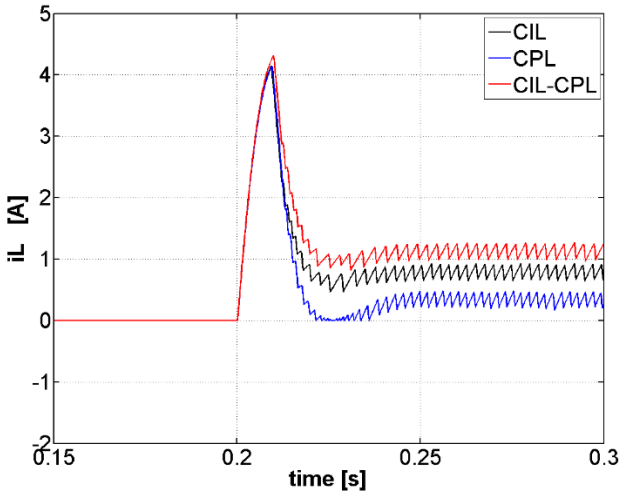

Figure 3.6. *Inductor currents for the three loads.*

The regulation of the DC-DC signals with various reference values allows for the identification of how the control system works and it is a good indicator to compare and find similitude among the different loads. Figures 7a and 7b show the output signal v_c for the different loads plotted against time. The tests were performed considering various steps in the reference signals as $v_{cref} = 10$ V in times between 0.05 and 0.1 s; $v_{cref} = 20$ V in times between 0.1 and 0.2 s; and $v_{cref} = 30$ V in times between 0.2 and 0.3 s. These figures show that the regulation is similar for cases when the reference signal is increased or reduced. There are some small differences in the response times and the maximum peaks of the signal, having a longer settling time for the system with a CPL load. In steady-state for the three tests, the error is lower than 4%. Figure 7b shows that the error is increased when the reference signal is close to zero. Therefore, the three tests in this research show that signals have similar regulation behaviors.

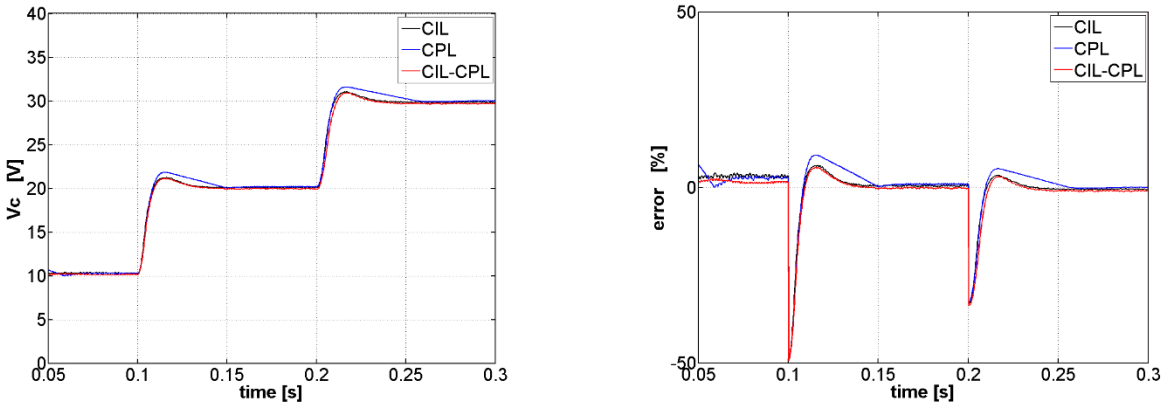

(**a**) output voltage v_c (**b**) error in v_c

Figure 3.7. *Behavior of the system for the three loads.*

3.3.2. Bifurcation Diagrams

The bifurcation diagram is useful in dynamical systems because it shows the possible long-term values of a system (fixed points or periodic orbits) as a function of a bifurcation parameter. Besides, bifurcation diagrams allow the identification of operation zones and the stability limits of the system. To draw the bifurcation diagrams, the system must reach the equilibrium point and the last values of the signal in steady-state operation are plotted. Figures 8a–8c show the output signals of the circuit v_c for the three tests. These figures have been plotted with MATLAB-Simulink and considering a k between 0 and 5 to identify the behavior of the circuit and compare the outputs for the three loads: CIL (40 Ω), CPL (10 watts), and CIL-CPL.

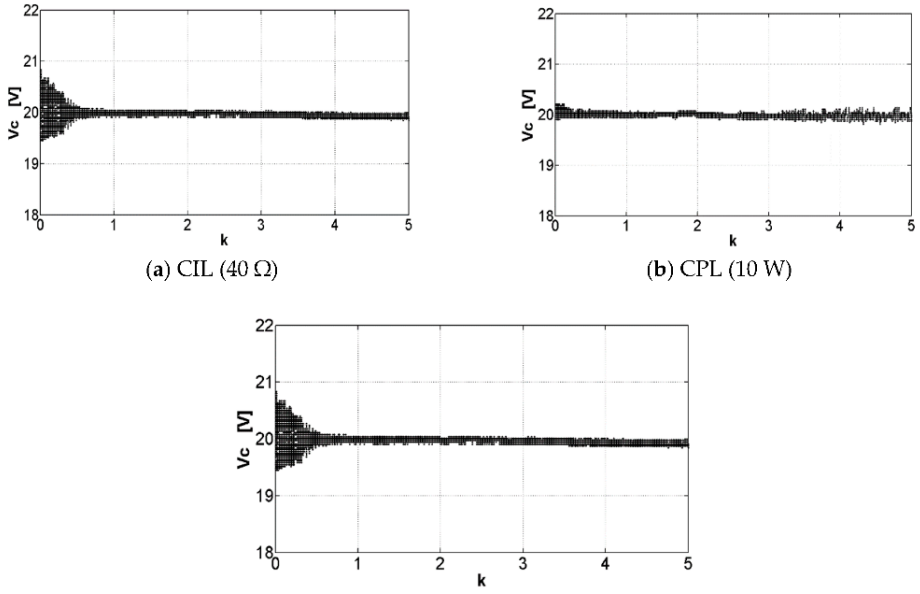

(a) CIL (40 Ω) (b) CPL (10 W)

(c) CIL (40 Ω) and CPL (10 W).

Figure 3.8. *Bifurcation diagram of Vc vs K.*

In these figures, similar behaviors in the output voltages are observed when the parameter k is increased. For k values greater than 0.5, voltages are close to the reference signal v_{cref}. For values lower than $k = 0.3,$ the voltages are a little different in magnitude, but the values tend to the reference voltage v_{cref}.

Figures 3.9a–3.9c show the errors obtained for the CIL, CPL, and CIL-CPL, respectively. The figures show that the system regulates with a greater steady-state error for all values of k. It is observed that the error is less than 2% for values of k greater than 0.5. However, the error is larger in the case where the load is CPL than for the other cases. From the figures, it is shown that a good choice of the parameter k to improve stability and regulation represents a value close to 0.8.

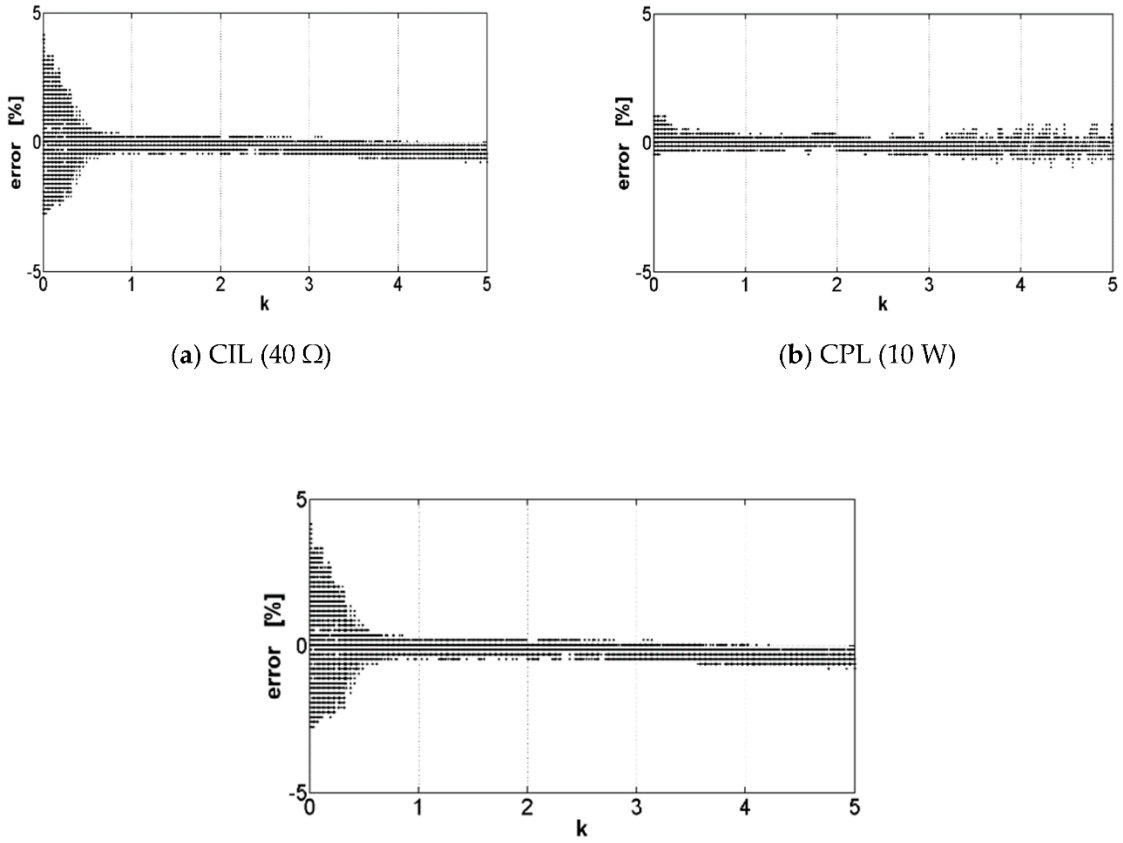

(**a**) CIL (40 Ω)

(**b**) CPL (10 W)

(**c**) CIL (40 Ω) and CPL (10 W).

Figure 3.9*. Bifurcation diagram of the error vs. K.*

3.3.3. Comparison of Different Controllers

To show the advantages of the control technique used in this investigation, comparisons among PID, conventional SMC, and SMC with washout filter are performed. The design of a PID controller and SMC, with the parameters of the buck converter, are explained in [17]. The results shown below are simulated in continuous time and some parameters have been changed with values such as $C = 46$ μF, $L = 2.47$ mH, and the switching frequency Fc = 20 kHz. As the parameters of the LC filter are smaller, they let signals of higher frequency to pass because the settling time in the continuous time is much less than the settling time in discrete time (Figures 5, 6, and 7), given in the previous results of this document.

Figure 3.10 shows the voltage v_c and error for the three controllers: PID, SMC, and SMC with washout filter. Besides, this figure shows the response of the controllers when the loads are only CILs. The voltage and error are shown in Figures 10a and 10b when CIL = 10 Ω and CPL = 0 watts; in Figures 10c and 10d when CIL = 25 Ω and CPL = 0 watts; and in Figures 10e and 10f when CIL = 50 Ω and CPL = 0 watts.

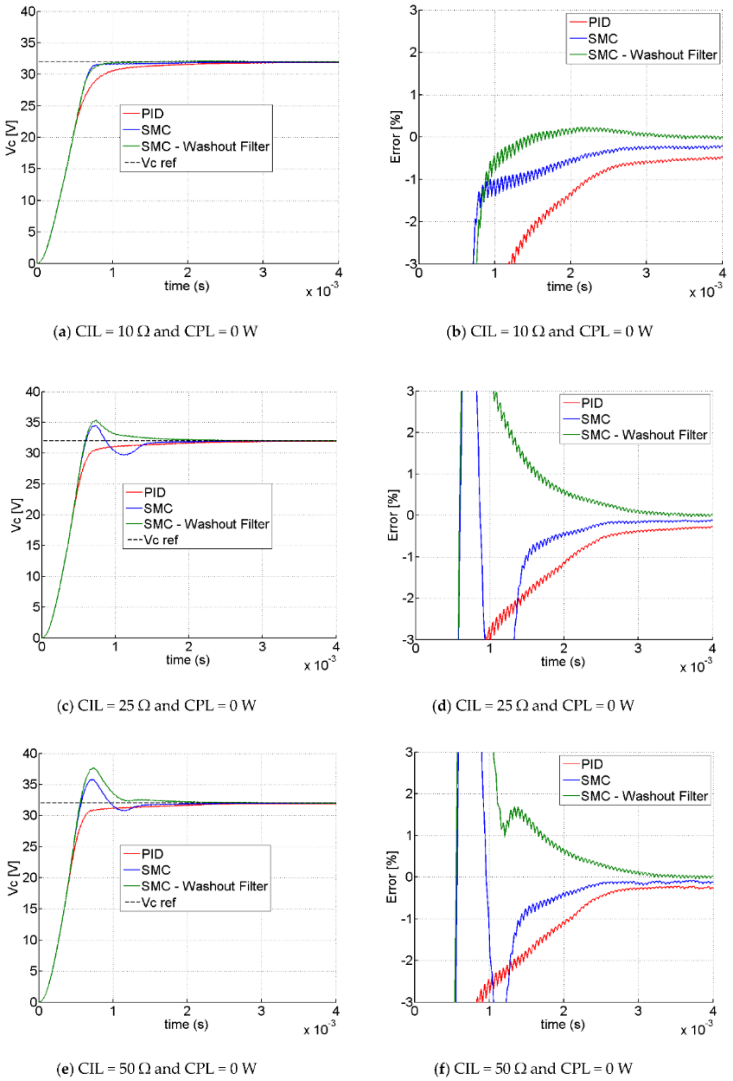

(a) CIL = 10 Ω and CPL = 0 W (b) CIL = 10 Ω and CPL = 0 W

(c) CIL = 25 Ω and CPL = 0 W (d) CIL = 25 Ω and CPL = 0 W

(e) CIL = 50 Ω and CPL = 0 W (f) CIL = 50 Ω and CPL = 0 W

Figure 3.10. *Voltage Vc and error for the CIL load and the three controllers: Proportional- integral-derivative (PID), sliding-mode control SMC, and SMC with washout filter.*

The settling time for the SMC with washout filter is close to 2.5 ms, for the PID it is 3 ms, and for the SMC it is 2.5 ms, which shows that they have similar behaviors. The highest overshoot is presented for the SMC with washout filter with a value of 17.6%. The smallest error is presented during the steady-state operation for the three loads when SMC with washout filter is used, which makes it more suitable for regulating voltage signals in this type of system; however, the three controllers have steady-state errors less than 0.5% for the different load values.

Figure 3.11 shows the voltage behavior v_c and error for the three controllers: PID, SMC, and SMC with washout filter. Besides, Figure 11 shows the response of the controllers when the loads are CIL and CPL. The voltage and error are shown in Figures 11a and 11b when CIL = 25 Ω and CPL = 40 watts; in Figures 11c and 11d when CIL = 25 Ω and CPL = 16 watts; and in Figures 11e and 11f when CIL = 25 Ω and CPL = 8 watts.

The settling time for the SMC with washout filter remains similar to that obtained previously and it is close to 2.5 ms. For both the PID and conventional SMC, the value of settling time obtained is around four times that obtained with the SMC with washout filter. Regarding the settling time, it can be concluded that the SMC with washout filter controller is capable of regulating the voltage faster when there are CPLs. The steady-state error for the three load variation tests shows that the SMC with washout filter behaves better than the other two controllers as the maximum error for the PID is close to 12%, for the conventional SMC it is 10%, and for the SMC with washout filter it is less than 2% when CIL = 25 Ω and CPL = 40 watts. For the other load variations tested, the error for the SMC with washout filter remains less than 1% and for the other controllers it is still greater than 2%.

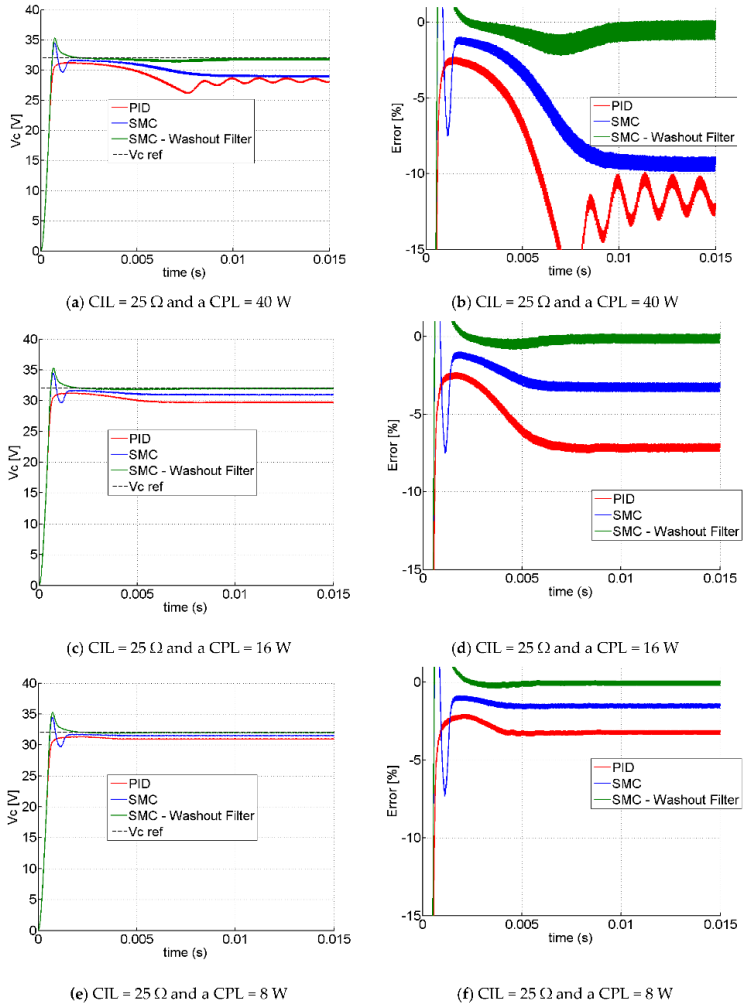

Figure 3.11. *Voltage* $\boldsymbol{v_c}$ *and error for the CIL-CPL loads and the three controllers: PID, SMC, and SMC with washout filter*

3.4. Conclusions.

This paper presented the nonlinear effects of an SMC based on a washout filter that considers CIL and CPL. For this purpose, an electronic circuit was modeled and simulated in MATLAB-Simulink to visualize the different nonlinear effects created when different types of loads are connected. The results show that the system regulates well the voltage with the three loads tested. The robustness of the system was checked by changing the control parameter k, obtaining a steady-state error less than 3%. Additionally, the quantization, system discretization, and delay effects

present in real systems were modeled to obtain results closer to those obtained with real circuits and that can be used in future research. A buck converter with a quasi-sliding control technique was placed as a CPL load, realizing that the system does not present unstable zones and a high steady-state error, and that the steady-state error is a little greater than the other two loads when the parameter k changes. From the bifurcation diagrams, it was observed that when the control parameter was around 0.5, the operation was close to the limit. Therefore, it is recommended to increase this value to avoid entering the zone where the steady-state error is greater. In the comparison of the performance of the three controllers with load variations, it was observed that the three controllers regulate well the voltage at the output with CIL; however, if the load is a combination of CIL and CPL, then the only controller that regulates well the voltage signal with small setting times and low steady-state error is the SMC with the washout filter.

Further research will analyze the SMC in an MG environment, integrating the controllers with other types of PCs as DC-AC. Future work will also consider the integration of the filter with the main control of the MG and compare the control efficiency with other methods. A classification of nonlinear effects can also be performed based on a bifurcation analysis to identify the effectivity of the response of the controller and the dynamic behavior. In addition, experimental validation of the dynamic responses of the SMC with the washout filter is required to validate the benefits of the controller. Finally, theoretical and experimental research with three-phase loads and various types of motors may be controlled by using an SMC with a washout filter.

References

1. *Venkataramanan, G.; Marnay, C. A larger role for microgrids. IEEE Power Energy Mag. 2008, 6, 78–82.*
2. *Badal, F.R.; Das, P.; Sarker, S.K.; Das, S.K. A survey on control issues in renewable energy integration and microgrid. Prot. Control Mod. Power Syst. 2019, 4, 8.*
3. *García Vera, Y.E.; Dufo-López, R.; Bernal-Agustín, J.L. Energy Management in Microgrids with Renewable Energy Sources: A Literature Review. Appl. Sci. 2019, 9, 3854.*
4. *Bouzid, A.M.; Guerrero, J.M.; Cheriti, A.; Bouhamida, M.; Sicard, P.; Benghanem, M. A survey on control of electric power distributed generation systems for microgrid applications. Renew. Sustain. Energy Rev. 2015, 44, 751–766.*
5. *Rocabert, J.; Luna, A.; Blaabjerg, F.; Rodríguez, P. Control of Power Converters in AC Microgrids. IEEE Trans. Power Electron. 2012, 27, 4734–4749.*
6. *Dragicevic, T.; Lu, X.; Vasquez, J.C.; Guerrero, J.M. DC Microgrids—Part II: A Review of Power Architectures, Applications, and Standardization Issues. IEEE Trans. Power Electron. 2016, 31, 3528–3549.*
7. *Dragicevic, T.; Lu, X.; Vasquez, J.C.; Guerrero, J.M. DC Microgrids–Part I: A Review of Control Strategies and Stabilization Techniques. IEEE Trans. Power Electron. 2015, 31, 4876–4891.*
8. *Bandyopadhyay, B.; Deepak, F.; Kim, K.S. Sliding Mode Control Using Novel Sliding Surfaces; Springer: Berlin, Germany, 2009; Volume 392.*
9. *Zinober, A.S.I. An introduction to sliding mode variable structure control. In Variable Structure and Lyapunov Control; Springer: London, UK, 1994; pp. 1–22.*
10. *Pagano, D.J.; Ponce, E. On the robustness of the DC-DC boost converter under washout SMC. In Proceedings of the 2009 Brazilian Power Electronics Conference (COBEP2009), Bonito-Mato Grosso do Sul, Brazil, 27 September–1 October 2009; pp. 110–115.*
11. *Tahim, A.P.N.; Pagano, D.J.; Ponce, E. Nonlinear control of dc-dc bidirectional converters in stand-alone dc Microgrids. In Proceedings of the 2012 IEEE 51st IEEE Conference on Decision and Control (CDC), Maui, HI, USA, 10–13 December 2012; pp. 3068–3073.*
12. *Tahim, A.P.N.; Pagano, D.J.; Heldwein, M.L.; Ponce, E. Control of interconnected power electronic converters in dc distribution systems. In Proceedings of the COBEP 2011—*

11th Brazilian Power Electronics Conference, Praiamar, Brazil, 11–15 September 2011; pp. 269–274.

13. *Kwasinski, A.; Onwuchekwa, C.N. Dynamic Behavior and Stabilization of DC Microgrids With Instantaneous Constant-Power Loads. IEEE Trans. Power Electron. 2011, 26, 822–834.*
14. *Zhao, Y.; Qiao, W.; Ha, D. A sliding-mode duty-ratio controller for DC/DC buck converters with constant power loads. IEEE Trans. Ind. Appl. 2014, 50, 1448–1458.*
15. *Grigore, V.; Hatonen, J.; Kyyra, J.; Suntio, T. Dynamics of a buck converter with a constant power load. In Proceedings of the PESC 98 Record. 29th Annual IEEE Power Electronics Specialists Conference, Fukuoka, Japan, 22–22 May 1998; Volume 1, pp. 72–78.*
16. *Hossain, E.; Perez, R.; Nasiri, A.; Padmanaban, S. A Comprehensive Review on Constant Power Loads Compensation Techniques. IEEE Access 2018, 6, 33285–33305.*
17. *AL-Nussairi, M.K.; Bayindir, R.; Padmanaban, S.; Mihet-Popa, L.; Siano, P. Constant power loads (CPL) with Microgrids: Problem definition, stability analysis and compensation techniques. Energies 2017, 10, 1656.*
18. *Hoyos, F.E.; Candelo-Becerra, J.E.; Toro, N. Numerical and experimental validation with bifurcation diagrams for a controlled DC–DC converter with quasi-sliding control. TecnoLógicas 2018, 21, 147–167.*
19. *Hoyos, F.; Candelo, J.; Silva, J. Performance evaluation of a DC-AC inverter controlled with ZAD-FPIC. INGE CUC 2018, 14, 9–18.*
20. *Ponce, E.; Pagano, D.J. Sliding Dynamics Bifurcations in the Control of Boost Converters*. IFAC Proc. Vol. 2011, 44, 13293–13298.*
21. *Hoyos, F.E.; Burbano, D.; Angulo, F.; Olivar, G.; Toro, N.; Taborda, J.A. Effects of Quantization, Delay and Internal Resistances in Digitally ZAD-Controlled Buck Converter. Int. J. Bifurc. Chaos 2012, 22, 1250245.*
22. *Fossas, E.; Griñó, R.; Biel, D. Quasi-Sliding control based on pulse width modulation, zero averaged dynamics and the L2 norm. In Proceedings of the Advances in Variable Structure Systems-6th IEEE International Workshop on Variable Structure Systems, Gold Coast, Australia, 7–9 December 2000; pp. 335–344.*
23. *Ashita, S.; Uma, G.; Deivasundari, P. Chaotic dynamics of a zero average dynamics controlled DC–DC Ćuk converter. IET Power Electron. 2014, 7, 289–298.*

24. *Hoyos, F.E.; Candelo-Becerra, J.E.; Hoyos Velasco, C.I. Model-Based Quasi-Sliding Mode Control with Loss Estimation Applied to DC–DC Power Converters. Electronics 2019, 8, 1086.*
25. *Hoyos, F.E.; Toro, N.; Garcés-Gómez, Y. Numerical and Experimental Comparison of the Control Techniques Quasi-Sliding, Sliding and PID, in a DC-DC Buck Converter. Sci. Tech. 2018, 23, 25–33.*

4. EXPERIMENTAL VALIDATION OF A NON-LINEAR SLIDING-MODE CONTROL BASED ON A WASHOUT FILTER APPLIED TO MICROGRIDS.

This article was published in the journal "International Review of Automatic Control" (IREACO) Vol13, N.4 ISSN 1974-6059 - DOI: https://doi.org/10.15866/ireaco.v13i4.17672.

Abstract

This paper presents an experimental validation of a non-linear sliding-mode control based on a washout filter when is submitted to alterations in the load, control parameter, and voltage reference. The numerical and the experimental tests are compared to visualize the non-linear effects caused by the power electronic converters and a comparison of the errors obtained for both test is presented. The results show that similar behaviors are presented in both cases with low error in the controlled variable vc. Furthermore, when representing bifurcations, both tests show similar behaviors, although the experimental test has a low displacement in the signal. This method is useful to monitor non-linear effects of micro grid and to design new filters or modify settings in the parameters.

4.1 Introduction.

The power demand continues increasing and now more distributed power generation is located close to the loads in the need of improving reliability of electrical networks. Renewable energies are now part of this distributed generation included under the concept of microgrids [1]-[3]. The use of power converters has turned the Direct Current (DC) circuits more efficient, allowing the creation of new architectures that help manage different type of loads [4]. However, many electronic transferring power from alternate current to direct current known as AC-DC power converters and from direct current to direct current known as DC-DC power converters are used

to supply the different types of power loads, creating instabilities events in the power grid that should be studied and controlled [5], [6]. From the study perspective of the microgrid stability, the problem can be divided from the feeder side, the intermediate circuits, and the load side. Therefore, the analysis also can be designed fulfilling those three points of view as shown in [7], likewise, modifying the impedance of the upstream circuit, adding auxiliary power circuits or modifying the input impedance [8]. Some authors have proposed the prevention of the instability of the constant power loads in distribution systems by using energy storage devices connected to the dc bus [4], [9]. Other one's deal with oscillation compensation techniques by using LC filter [10]. The division into two operation modes has been also analyzed: constant voltage source mode and droop mode reducing the problem to an eigenvalue problem [11]. The load shedding technique has been also used to stabilize the oscillations in the system [12]. The previous solutions presented in literature are provided as solutions to the problem; load shedding is not an option for all the events presented in the distribution system and filters are expensive to invest in all the cases presented in the system [13], [14]. Even though, Sliding-Mode Control (SMC) is not a novel technique, it is still a successful method handling uncertainties and complex dynamics [25]-[30]. SMC controllers for converters with Constant Power Loads have been proposed [15], [16]-[19], some controllers are combined with washout filters [11], [13], [20] and some other SMC with self-optimizing for PV applications [21]. This is an adequate solution to control the voltage in the output bus regarding the load variation.

However, the representation of the different effects by using the emulation of the non-linear effects is still needed, besides the different behavior of the changes that can be created in the electrical circuit. Furthermore, a real-time evaluation can be represented with the circuit in order to monitor the behavior of the loads. Likewise, other experimental approaches have been developed aiming to stabilize DC bus with

SMC control via storage charge-discharge and giving satisfactory results in terms of time and voltage regulation and some disadvantages regarding overvoltage due to current transients [22]. Some advantages of the control technique are shown in [23], where comparisons among PID, conventional SMC, and SMC with washout filter have been performed. After generating changes in the load that considers a CIL, the three controllers regulate well the voltage at the output; however, when the load is a combination of CIL and CPL, the controller with the washout filter is the only one to regulate well the voltage signal with small setting times and low steady-state error. This paper presents the experimental validation of non-linear effects that constant loads produce in a micro grid.

The experiment consisted on changing the values of CIL to evaluate the robustness of the control; besides the voltage regulation has been changed in the output bus to minimize the transient response according to load changes. The model includes MOSFET resistance, inductor internal resistance, measurement resistance, power source resistance, diode voltage, and the quantization of the state variables and duty cycle due to Analog to Digital Converter, which allow obtaining signals that are more precise, are represented in the experimental test. Finally, a numerical bifurcation has been performed by changing the parameters k and w, with the aim of visualizing the non-linear effects of the circuit and the load. All these tests have been validated by measuring the voltage in the output bus v_c.

Thus, the rest of the document is divided into three sections. Section II presents the materials and the methods used in this research with the mathematical fundamentals, the simulations, and the electronic circuit implemented to visualize the stability effects and control. Section III presents the results, the analysis, and the discussions obtained from the experiments. Finally, Section IV considers conclusions and suggests probable future research.

4.2 Material and Methods.

This section includes the electrical network architecture, the load models connected to the network, the equivalent circuit to study, the washout filter, the sliding control mode, the electrical circuit consider for the validation, and the tests designed to proof the representation of different events presented in the network.

4.2.1. General Methodology.

The test consisted of creating an electronic circuit that emulates the effects of a micro-grid system with different load variations. Then, an analysis of the effects of the changes in the network was executed. Finally, bifurcation diagrams are constructed with the simulated system and with the system in real time.

4.2.2. Micro Grid Architecture.

Some micro grids use renewable energies and the power grid to supply the demand, the maintaining controllability, the reliability, and the efficiency. One of these micro grid architectures uses AC-DC and DC-DC power converters, as represented in Fig. 4.1 [13]. In this figure, DC-DC converters are used to connect sources as photovoltaic panels and batteries to the input bus; AC- DC converters are used to connect wind generators and a power grid to the input bus. Another stage considers a regulating buck converter that connects the system to a constant impedance load. This type of load can create different non-linear effects on the systems, which are analyzed in this paper with a circuit that generates real-time signals representing the non-linear effects and compared to the responses of a simulated model.

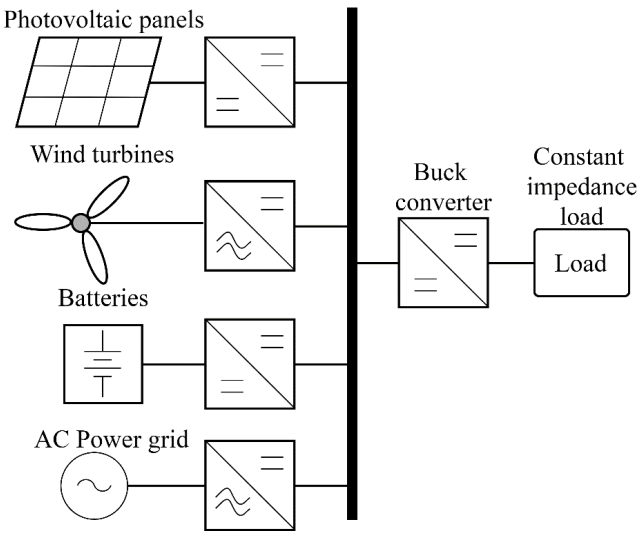

Figure 4.1. *Simplified DC power network.*

4.2.3. Simplified Model of the Network.

Fig. 4.2 shows a representation of the DC distribution network implemented to analyze the different effects of the load variation.

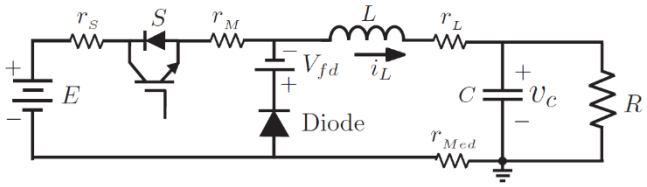

Figure 4.2. *Circuit model of the Buck power converter.*

This figure presents the diagram of the buck converter with the resistance connected to the output. The converter has a power source with voltage E, the internal source resistor r_s, a Metal-Oxide-Semiconductor Field-Effect Transistor (MOSFET) working as a switch S, an internal MOSFET resistance r_M, a diode D with Forward voltage diode V_{fd}, a filter LC, an internal resistance of the inductor r_L, a resistance used to measure current r_{Med}, and a resistance representing the load of the circuit R.

Fig. 4.3 shows the diagram of the Digital PWM controller connected to the buck converter and the sensors used to measure the different input signals. Besides, a washout filter and a sliding mode controller are used to regulate the output signal. The response to the dynamics created according to the variation of the resistance load can be regulated by this sliding mode control.

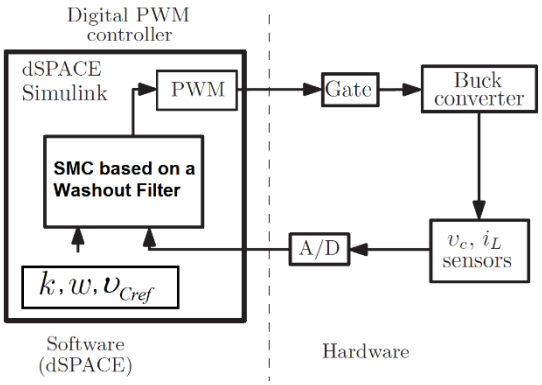

Figure 4.3. *Block diagram of the experiment.*

This circuit has been used to represent the mathematical and the numerical models that are solved to identify the variations and the response of the system. Besides, a real electronic circuit that represents the same effects of theoretical and simulation models has been created to validate the stabilization responses of the sliding mode control with the washout filter. The bifurcations diagrams obtained from the simulation and the experimental have also been compared to identify the behaviors.

4.2.4. Mathematical Model.

The load use for the investigation is related to the use of the resistance load shown in Fig. 4.2 and the representation of the impedance behavior. Then, the current supplied by the electrical circuit is defined as in Eq. (4.1):

$$i_{dc} = \frac{v_c}{R} \qquad (4.1)$$

Where R is the constant resistance in the load, the P is the constant power of the load, and v_c is voltage of the capacitor. The equivalent resistance of the circuit can be obtained according to the voltage and the current in the bus, as expressed in Eq. (4.2):

$$R_{eq} = \frac{v_c}{i_{bus}} \qquad (4.2)$$

4.2.5. Dynamic of Buck Converter PC1.

The dynamics of a buck converter model feeding a Constant Impedance Load (CIL) Eq. (4.2) can be represented as Eq. (4.3) and Eq. (4.4). When the control input is $u = 1$, then the state of the switch S is active (ON) and the system gets into a continuous conduction mode (CCM), which can be modeled as in Eq. (4.3).

$$\begin{bmatrix} \dot{v}_C \\ \ddot{i}_L \end{bmatrix} = \begin{bmatrix} -\frac{1}{RC} & \frac{1}{C} \\ -\frac{1}{L} & \frac{-(r_s+r_M+r_{Med}+r_L)}{L} \end{bmatrix} \begin{bmatrix} v_C \\ i_L \end{bmatrix} + \begin{bmatrix} 0 \\ \frac{E}{L} \end{bmatrix}. \qquad (4.3)$$

When the control input is $u = 0$, switch S is inactive (OFF) and the system can be modeled as shown in Eq. (4.4).

$$\begin{bmatrix} \dot{v}_C \\ \ddot{i}_L \end{bmatrix} = \begin{bmatrix} -\frac{1}{RC} & \frac{1}{C} \\ -\frac{1}{L} & \frac{-(r_{Med}+r_L)}{L} \end{bmatrix} \begin{bmatrix} v_C \\ i_L \end{bmatrix} + \begin{bmatrix} 0 \\ \frac{-v_{fd}}{L} \end{bmatrix}. \qquad (4.4)$$

The solution for the Discontinuous Conduction Mode (DCM) is given by Eq. (4.5) and Eq. (4.6) and it occurs when the current in the inductor is equal to zero:

$$\frac{di_L}{dt} = 0 \qquad (4.5)$$

$$C\frac{dv_c}{dt} = -\frac{v_c}{R} \qquad (4.6)$$

4.2.6. Voltage Measurement.

The voltage in the bus 2 can be measured and used as an input for the sliding mode controller. This can be represented as v_m and is equal to the voltage at the bus 2 and the capacitor voltage.

$$v_m = v_c = V_{bus2} \qquad (4.7)$$

This value will be changed according to the regulation of the sliding mode controller with washout filter. The final voltage magnitude depends on the voltage references given for the controller and the regulation limits allowed by the circuit. This is a part of the test to be conducted in this research with the real-time signals provided by the circuits with the changes in loads.

4.2.7. Washout Filter.

This method consists of passing the inductor current, i_L, through a washout filter, as shown in Fig. 4.3. After the filter with a transfer function, we obtain a final signal called i_F. The transfer function, G_F, that is used to a new filtered current is expressed in Eq. 4.8; where, the s is the Laplace expression, w is the cut-off frequency of the high-pass filter, i_F represents the filtered inductor current created.

$$G_F(s) = \frac{I_F(s)}{I_L(s)} = \frac{s}{s+w} = 1 - \frac{w}{s+w} \qquad (4.8)$$

After the induction current is filtered, a differential equation is created and added to the model, as expressed in Eq. 4.9. Where z corresponds to the difference between the current of i_L and i_F.

$$\frac{dz}{dt} = w(i_L - z) \qquad (4.9)$$

4.2.8. Sliding Mode Controller.

The circuit of the Fig. 4.3 has a sliding mode control that receives two signals, v_c that corresponds to the capacitor voltage and i_F that is the filtered inductor control coming from the washout filter. Then, a control law is applied to determine the final output signal, depending on two switching stages, as shown in Eq. 10. Where, u is a scalar that depends on x, and can take to values u^-=0 and u^+=1. Thus, two conditions are presented depending on the conditions of the output of the function $h(x)$, with x=i_L, v_c, z.

$$u = \begin{matrix} \{u^- = 0, \\ \{u^+ = 1, \end{matrix} \quad \begin{matrix} if \\ if \end{matrix} \quad \begin{matrix} h(x) > 0 \\ h(x) < 0 \end{matrix} \qquad (4.10)$$

Then the sliding mode controller has the answer $h(x)$, with the following expression Eq. 4.11. Where, v_c corresponds to the capacitor voltage, v_{cref} is the voltage reference required to regulate the system, i_L is the inductor current and z the current difference obtained in the output of the circuit. The term k is a parameter used in the controller that multiply the filtered current and takes values greater than zero (k>0). This parameter k can be adjusted in the controller to obtain the different responses of the system and it will be changed to identify the dynamics of the system.

$$h(x) = v_c - v_{cref} + k(i_L - z) = 0 \qquad (4.11)$$

The continuous conduction mode of the system is presented considering Eq. (4.12). First, when the switch is in the state on, then the resulting equations of current, the voltage, and z are shown in Eq. (4.12):

$$f^{+}(x) = \begin{bmatrix} \dot{v}_c \\ \dot{i}_L \\ \dot{z} \end{bmatrix}_{u=1} = \begin{bmatrix} \frac{-1}{RC} v_c + \frac{1}{C} i_L \\ \frac{-1}{L} v_c - \frac{r_S + r_M + r_{Med} + r_L}{L} i_L + \frac{E}{L} \\ \omega(i_L - z) \end{bmatrix} \qquad (4.12)$$

Then, when the switch is off, a vector field is presented with the new equations of the inductor current, capacitor voltage and z [24], as shown in Eq. (4.13):

$$f^{-}(x) = \begin{bmatrix} \dot{v}_c \\ \dot{i}_L \\ \dot{z} \end{bmatrix}_{u=0} = \begin{bmatrix} \frac{-1}{RC} v_c + \frac{1}{C} i_L \\ \frac{-1}{L} v_c - \frac{r_{Med} + r_L}{L} i_L + \frac{V_{fd}}{L} \\ \omega(i_L - z) \end{bmatrix} \qquad (4.13)$$

The presented test has consisted of validating this stability for the different parameters of the load and k, the response of the sliding mode controller with washout filter and determining the numerical bifurcations in the system.

4.2.9. Numeric Algorithm.

Fig. 4.4. shows a complete diagram implemented in Matlab-Simulink to control the buck converter using the SMC with the washout filter. The quantization effects are included as 12 bits for the voltage in the condenser v_c and the current in the inductor i_L. Besides, a delay period was included in the numerical simulation as the experimental test a delay period equal to 1/Fs is presented. The zero-order-hold block is necessary to simulate the fixed sample time and obtain v_c and i_L, calculating

u with Eq. 10. All the parameters of the buck converter and the SMC controller are shown in Table 4-1.

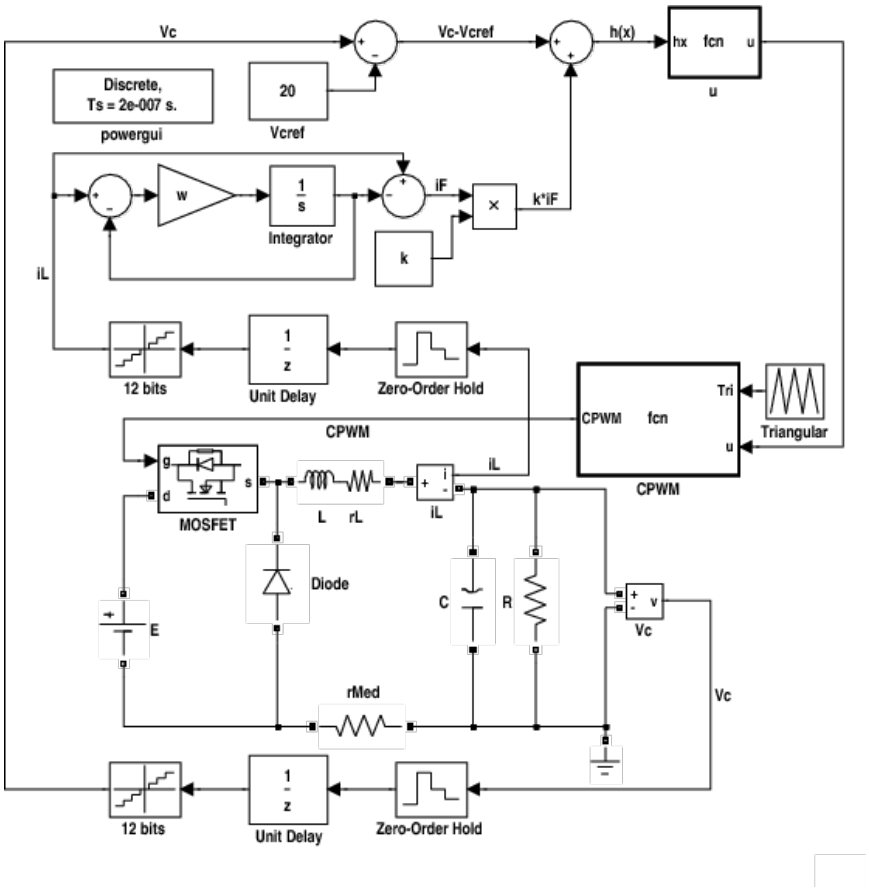

Figure 4.4. *Diagram of the global system.*

Parameter	Description	Value
R	Resistance of the load	20.44, and 40.092 Ω
C	Capacitance	938 μf
L	Inductance	53.35 mH
r_L	Internal resistance of the inductor	1.33 Ω
r_{Med}	Sensor resistance	1.007 Ω
r_M	Internal resistance of the MOSFET	0.3 Ω
r_s	Internal resistance of the source	0.3 Ω
E	Input voltage	40V (Dual source)

Fc	Commutation frequency	variable
Fs	Sampling frequency	40 kHz
k	Control parameter	1
w	Cut-off frequency high-pass filter	$w = 0.6\frac{1}{\sqrt{LC}}$

Table 4-1. *Parameters used in the DC test.*

4.2.10. Diagram of the Real-Time Control System

An electronic circuit was built with similar components as in the model defined for the simulation test, which helps to represent the real-time response in the experimental test. Fig. 4.5 shows the program developed in MATLAB-Simulink to execute the controller in real time with the use of a board DS1104 of dSPACE company. To acquire the values some ADC blocks are used, the channel 5 for the voltage v_c and channel 7 for the current i_L. In this program the slipping surface is calculated as $h(x) = v_c - v_{cref} + ki_F$. Then, if $h(x) > 0$ $u = 1$ and if $h(x) < 0$ $u = 0$. Finally, a block is required to generate the output PWMC.

A Hall effect-based linear current sensor was used to capture the dynamics of the system by considering a resistance less than 1.2 mΩ. However, as the sensor causes a loss of current dynamics when comparing to those obtained with the numerical tests, then a resistance of 1.007 Ω was used to capture all the dynamics and minimize the external electrical noise presented in the i_L.

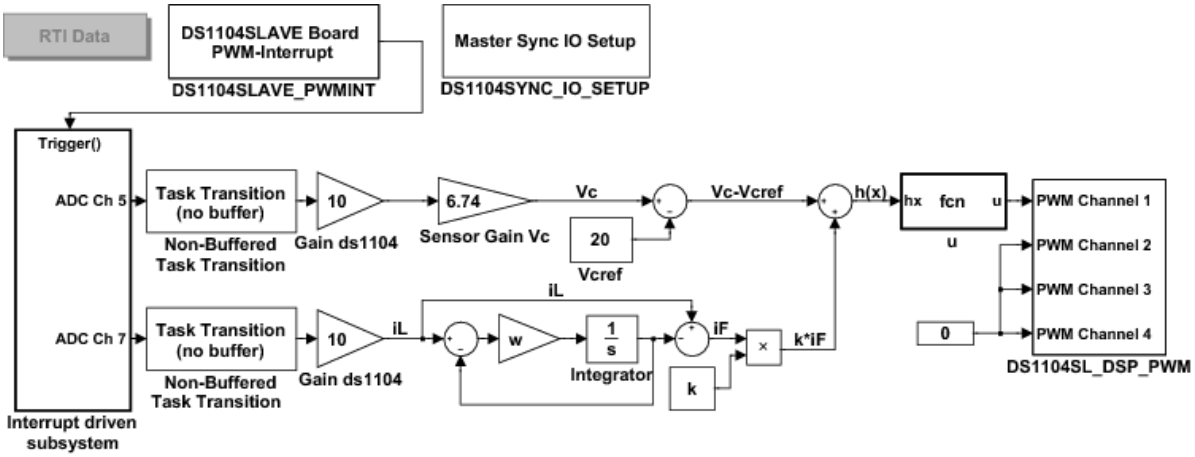

Figure 4.5. *Diagram of the circuit implemented in Matlab Simulink for real time control.*

4.3 Results and Analysis.

The following results show the validation of the non-linear sliding-mode control based on a washout filter for variations of load, voltage reference, and control parameter (k). The results are organized to show the robustness of the control, the voltage regulation, and the transient response of the controller.

4.3.1. Regulation of DC-DC Signals.

The comparisons between the simulation and the experimental tests allow us to determine similarities in the circuits and help to identify the real-time behavior of the system. The main comparison can be made in DC-DC regulation with a voltage reference (υ_{cref}). Fig. 4.6 shows the behavior of the output voltage υ_c, regulated with the control, plotted in the time for the simulation and experimental tests. These curves were created with the factor $k = 4$ and the voltage reference of $\upsilon_{cref} = 20$ V.

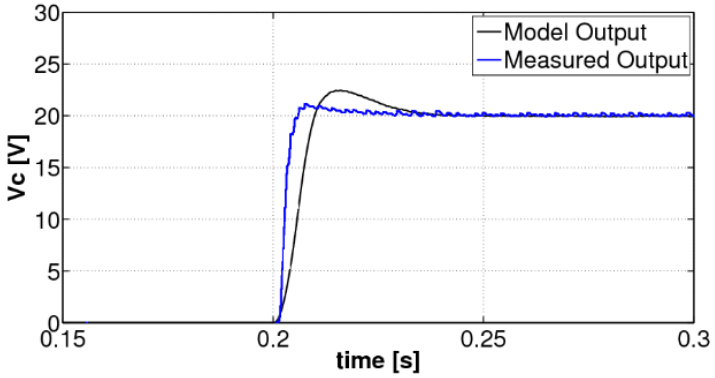

Figure 4.6. *Simulated and experimental tests with k=1 and voltage regulation of Vcref =20V.*

Both figures show that the behavior in the voltage signals are similar and after starting the signal and close to the 0.2 seconds, the voltage is regulated with a pick voltage magnitude that is later regulated to a voltage reference of 20 V and settling time of 0.25 seconds, the overshoot is 5 % for the experiment and 12.5 % for the simulation, rise time is smaller for the experimental case. Therefore, both adjusted circuits show similar responses with the control and that is a good indicator to conduct the different experiments. It is also important to identify the errors that are generated in the regulated signals of the system to identify similitude in the behaviors of the control. Fig. 4.7 shows errors in the signals for the simulation and experimental tests. These curves were created with the factor k=4 and the voltage reference of $v_{cref} = 20$ V. From both figures, the errors obtained for the voltage signals are similar.

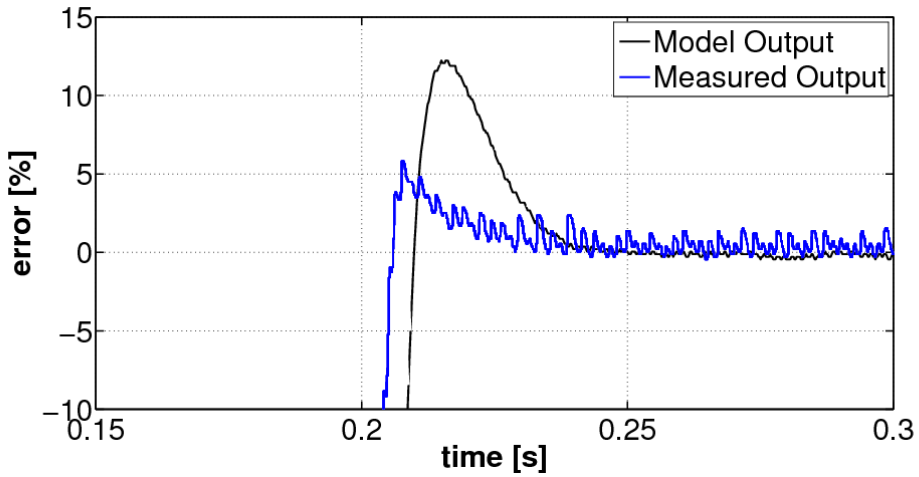

Figure 4.7. *Error in the regulation signal Vcref =20V for the experiment test.*

However, in the transient state the simulated signal shows a higher error compared to the value obtained with the experimental test. Besides, it is observed that the errors are reduced, and the values return to zero in similar times and close to 0.25 seconds in the steady state the error is lower than 2 %, for the numerical and experimental tests. Therefore, both tests show that there is a lot of similarity in the control, and it is a good indication to obtain different experimental results that are presented in the document.

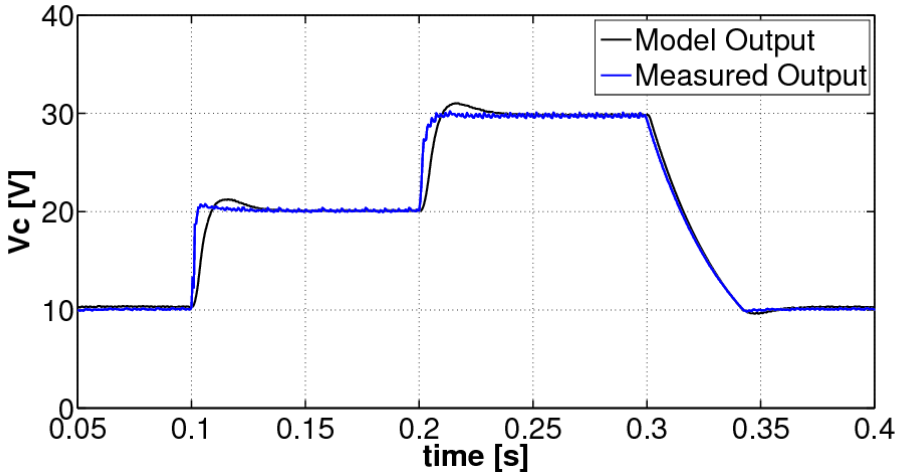

Figure 4.8. *Output voltage Vc for the experiment test.*

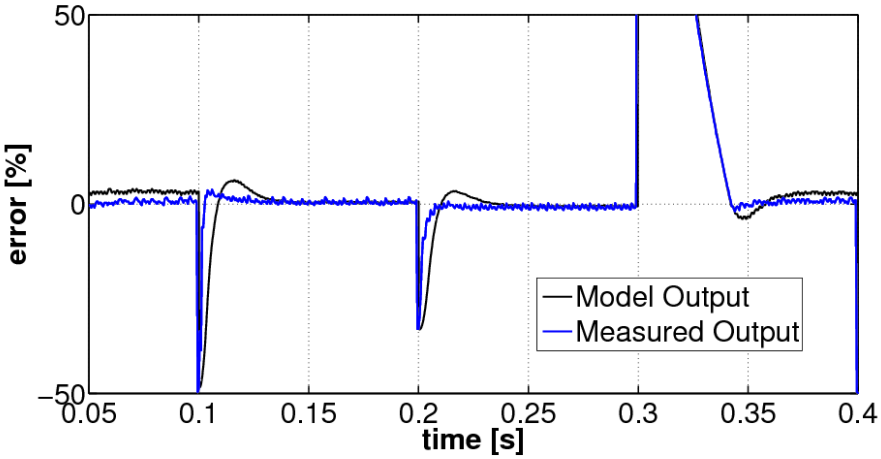

Figure 4.9. *Error for the regulation of various signals.*

The regulation of the DC-DC signals with various reference values allows us to identify the way that the control system works and it is a good indicator to compare and find similitude between the simulation and experimental tests. Figures 4.8 and 4.9 show the output signal v_c for the simulation and experimental tests plotted in the time. The test was performed considering various steps in the references signals as $v_{cref} = 10$ volts in times between 0.05 and 0.1 s; $v_{cref} = 20$ volts in times between 0.1 and 0.2 s; and $v_{cref} = 30$ volts in times between 0.2 and 0.3 s. These figures show that the regulation is similar for cases when the reference signal is increased or reduced. There are some small differences in the response times and the maximum peaks of the signal, being the data obtained with the circuit in experimental form faster for the response and the stabilization time than the steady state error presented in the simulation test. For the steady state, in both numerical and experimental tests, the error is lower than 3 %. Figure 4.9 shows that the error is increased when the reference signal is close to zero. Therefore, both circuits implemented in this research show that signals have similar regulation behaviors.

4.3.2. Robustness Test with Load Changes.

To identify that the system regulates the signals correctly when the load is changed, some robustness tests are performed. Figure 4.10 shows the output signal v_c for the numerical and experimental tests when load is variated. These changes are performed at $t = 0.2$ seconds when the load change from $R = 20.44\,\Omega$ to $R = 40.092\,\Omega$. Load variations show that the behavior of both circuits tested are similar to the load variation. This demonstrates that the load variation the voltage signals change and the system can stabilize fast the signals, having similar behavior both circuits. It is observed in these results that a larger overshoot is presented in the simulation than in the experimental test and that the signal is stabilize faster for the experimental test than the simulation test. The regulation continues to be acceptable with a low error of 3 % and the electric noise of the signals that is commonly presented in the experimental test were not model for the simulation test.

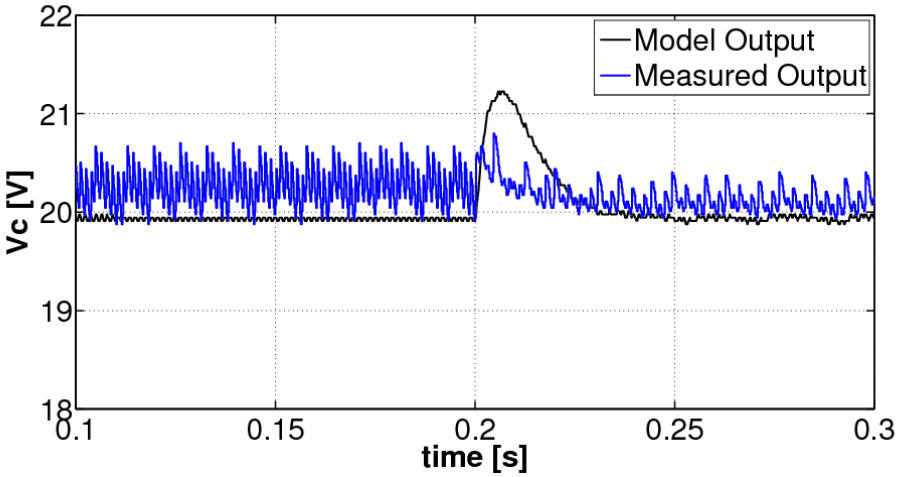

Figure 4.10. *Experimental test: Vc when the load is varied at t=00.2 from R=20.44 Ω to R=40.092 Ω.*

4.3.3. Bifurcation Diagrams.

The bifurcation diagram allows to identify the operation zones of the circuit and the stability limits of the system. Figures 4.11 and 4.12 show the output signals of the circuit v_c, for the simulation and experimental test, these figures have been plotted with a k between 0 and 5 to identify the behavior of the circuit and compare the output of both simulation and experimental test.

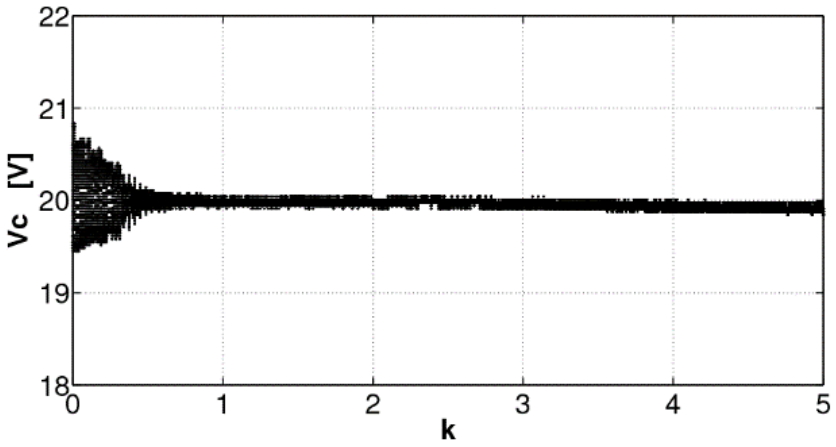

Figure 4.11. *Bifurcation diagram of Vc vs k for the simulation test.*

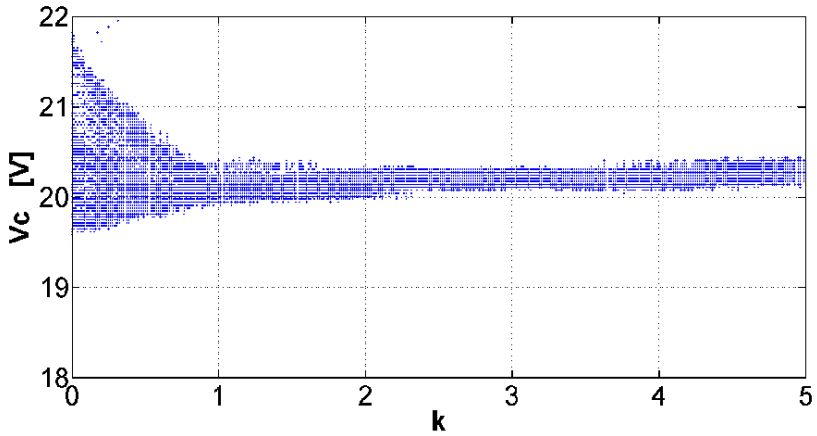

Figure 4.12. *Bifurcation diagram of Vc vs k for the experimental test.*

Both figures show similar behaviors in the response for the output voltages when the parameter k is increased. For k values greater than 1, the voltages are close to the reference signal v_{cref}. For values lower than $k = 0.5$ the voltages are a little different in magnitude, but its values tend to the reference voltage v_{cref}.

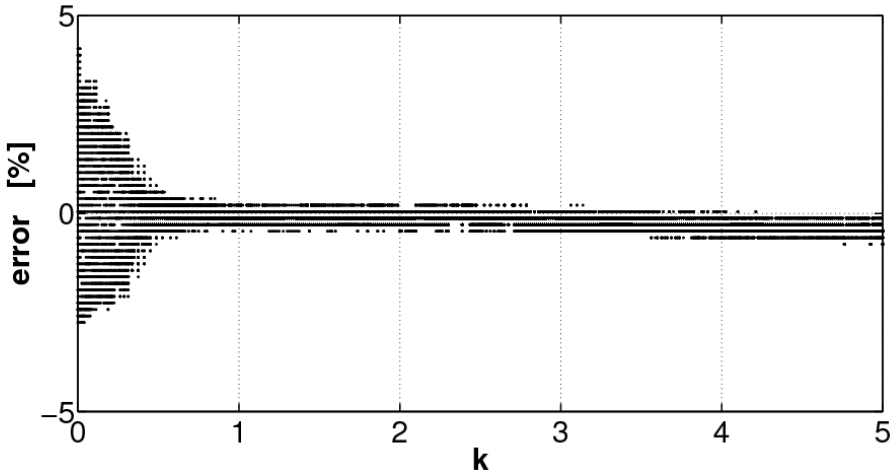

Figure 4.13. *Bifurcation diagram of the error vs k for the simulation test.*

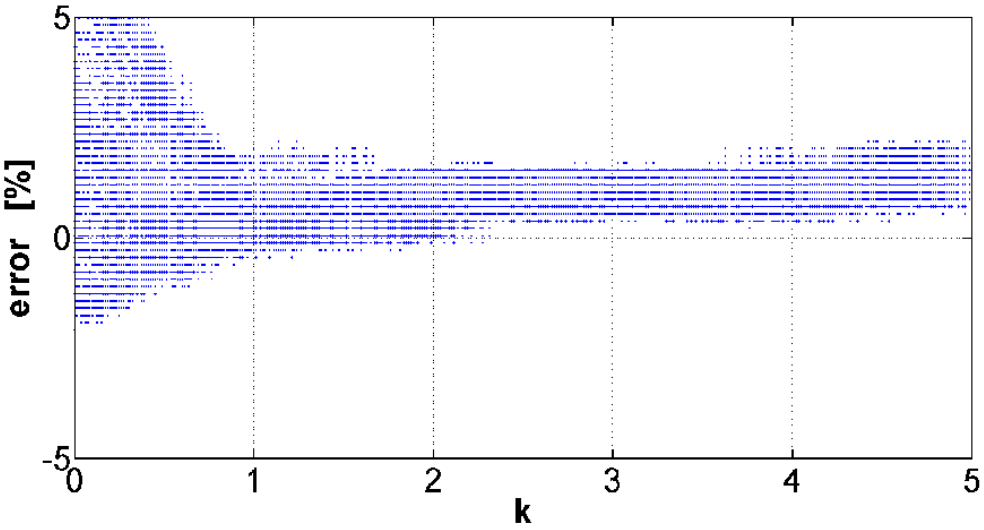

Figure 4.14. *Bifurcation diagram of the error vs k for the experimental test.*

Figures 4.13 and 4.14 show the errors obtained with the simulation and experimental tests, respectively. This figure was created in the same way than the previous ones, by changing the control parameter k. It is observed that the error at numerical and experimental level is less than 3% for values of k greater than 1. However, errors are larger in the experimental test when k approaches zero. From the figures Figures 11, 12, 13 and 14 it is concluded that a good choice of the parameter k would be a value close to 2 for better stability and good regulation.

4.4 Conclusions.

This paper has presented a real-time validation method of a non-linear sliding mode control based on a washout filter for identifying the destabilizing non-linear effects of power electronic converters. For this purpose, a circuit that emulates the effects caused by the power electronic converters according to the load changes has been presented to visualize the different destabilizing non-linear effects with different type of loads. The results have shown that the circuit reproduces all the events presented in the system with accuracy, the control is robust and regulates well the voltage at the output bus. The system presents many unstable events that have been reproduced and can be analyzed with the circuit. Furthermore, the bifurcation analysis of the system regarding k parameter and the availability has been presented.

From the bifurcation diagrams, it is observed that the system with the control parameters k is close to 1, the operation system is in the limit when performing the experimental test. Therefore, it is recommended to increase this value to avoid entering in the zone where the steady-state error is greater and the value of k must not increase too much because the output voltage v_c over passes the reference signal v_{cref} and the steady-state error is positive and tends to be higher with the increase of k.

In future work, the focus will be on identifying the different bifurcations with the electronic circuit that represents the real-time signals obtained from the circuit through different changes in the network, the control parameters, and the loads.

References

[1] G. Venkataramanan and C. Marnay, A larger role for microgrids, IEEE Power Energy Mag., vol. 6, no. 3, pp. 78–82, May 2008. doi: 10.1109/MPE.2008.918720.

[2] Y. Xu, C.-C. Liu, K. P. Schneider, F. K. Tuffner, and D. T. Ton, Microgrids for Service Restoration to Critical Load in a Resilient Distribution System, IEEE Trans. Smart Grid, vol. 9, no. 1, pp. 426–437, Jan. 2018. doi: 10.1109/TSG.2016.2591531.

[3] S. K. Sahoo, A. K. Sinha, and N. K. Kishore, Control Techniques in AC, DC, and Hybrid AC–DC Microgrid: A Review, IEEE J. Emerg. Sel. Top. Power Electron., vol. 6, no. 2, pp. 738–759, Jun. 2018. doi: 10.1109/JESTPE.2017.2786588.

[4] I. Gadoura, V. Grigore, J. Hatonen, J. Kyyra, P. Vallittu, and T. Suntio, Stabilizing a telecom power supply feeding a constant power load, in INTELEC - Twentieth International Telecommunications Energy Conference (Cat. No.98CH36263), pp. 243–248. doi: 10.1109/INTLEC.1998.793506.

[5] R. W. Erickson, D. Maksimović, R. W. Erickson, and D. Maksimović, Converter Circuits, in Fundamentals of Power Electronics, Springer US, 2001, pp. 131–184.

[6] Q. Xu, C. Zhang, C. Wen, and P. Wang, A Novel Composite Nonlinear Controller for Stabilization of Constant Power Load in DC Microgrid, IEEE Trans. Smart Grid, vol. 10, no. 1, pp. 752– 761, Jan. 2019. doi: 10.1109/TSG.2017.2751755.

[7] E. Hossain, R. Perez, A. Nasiri, and S. Padmanaban, A Comprehensive Review on Constant Power Loads Compensation Techniques, IEEE Access, vol. 6, pp. 33285–33305, 2018. doi: 10.1109/ACCESS.2018.2849065.

[8] M. WU and D. D.-C. LU, Active stabilization methods of electric power systems with constant power loads: a review, J. Mod. Power Syst. Clean Energy, vol. 2, no. 3, pp. 233–243, Sep. 2014. doi: 10.1007/s40565-014-0066-y.

[9] S. Pang et al., Interconnection and Damping Assignment Passivity-Based Control Applied to On-Board DC–DC Power Converter System Supplying Constant Power Load, IEEE Trans. Ind. Appl., vol. 55, no. 6, pp. 6476–6485, Nov. 2019. doi: 10.1109/TIA.2019.2938149.

[10] P. Liutanakul, A.-B. Awan, S. Pierfederici, B. Nahid-Mobarakeh, and F. Meibody-Tabar, Linear Stabilization of a DC Bus Supplying a Constant Power Load: A General Design Approach, IEEE Trans. Power Electron., vol. 25, no. 2, pp. 475–488, Feb. 2010. doi: 10.1109/TPEL.2009.2025274.

[11] M. Su, Z. Liu, Y. Sun, H. Han, and X. Hou, Stability analysis and stabilization methods of DC microgrid with multiple parallel- connected DC-DC converters loaded by CPLs, IEEE Trans. Smart Grid, vol. 9, no. 1, pp. 132–142, Jan. 2016. doi: 10.1109/TSG.2016.2546551.

[12] R. S. Balog, W. W. Weaver, and P. T. Krein, The Load as an Energy Asset in a Distributed DC SmartGrid Architecture, IEEE Trans. Smart Grid, vol. 3, no. 1, pp. 253–260, Mar. 2012. doi: 10.1109/TSG.2011.2167722.

[13] A. P. N. Tahim, D. J. Pagano, M. L. Heldwein, and E. Ponce, Control of interconnected power electronic converters in dc distribution systems, in XI Brazilian Power Electronics Conference, 2011, pp. 269–274. doi: 10.1109/COBEP.2011.6085269.

[14] A. Kwasinski and C. N. Onwuchekwa, Dynamic Behavior and Stabilization of DC Microgrids With Instantaneous Constant- Power Loads, IEEE Trans. Power Electron., vol. 26, no. 3, pp. 822–834, Mar. 2011. doi: 10.1109/TPEL.2010.2091285.

[15] S. Singh and D. Fulwani, Constant power loads: A solution using sliding mode control, in IECON Proceedings (Industrial Electronics Conference), 2014, pp. 1989–1995. doi: 10.1109/IECON.2014.7048775.

[16] V. Stramosk and D. J. Pagano, Nonlinear control of a bidirectional dc-dc converter operating with boost-type Constant- Power Loads, in 2013 Brazilian Power Electronics Conference, COBEP 2013 - Proceedings, 2013, pp. 305–310. doi: 10.1109/COBEP.2013.6785132.

[17] U. K. Kalla, B. Singh, S. S. Murthy, C. Jain, and K. Kant, Adaptive Sliding Mode Control of Standalone Single-Phase Microgrid Using Hydro, Wind, and Solar PV Array-Based Generation, IEEE Trans. Smart Grid, vol. 9, no. 6, pp. 6806– 6814, Nov. 2018. doi: 10.1109/TSG.2017.2723845.

[18] W. Qi, S. Li, S.-C. Tan, and S. Y. R. Hui, Parabolic-Modulated Sliding-Mode Voltage Control of a Buck Converter, IEEE Trans. Ind. Electron., vol. 65, no. 1, pp. 844–854, Jan. 2018. doi: 10.1109/TIE.2017.2716859.

[19] B. A. Martinez-Treviño, A. El Aroudi, E. Vidal-Idiarte, A. Cid- Pastor, and L. Martinez-Salamero, Sliding-mode control of a boost converter under constant power loading conditions, IET Power Electron., vol. 12, no. 3, pp. 521–529, Mar. 2019. doi: 10.1049/iet-pel.2018.5098.

[20] A. P. N. Tahim, D. J. Pagano, and E. Ponce, Nonlinear control of dc-dc bidirectional converters in stand-alone dc Microgrids, in 2012 IEEE 51st IEEE Conference on Decision and Control (CDC), 2012, pp. 3068–3073. doi: 10.1109/CDC.2012.6426298

[21] Y. M. Alsmadi et al., Sliding mode control of photovoltaic based power generation systems for microgrid applications, Int. J. Control, pp. 1–12, Jan. 2020. doi: 10.1080/00207179.2019.1664762.

[22] C. A. Ramos-Paja, J. D. Bastidas-Rodríguez, D. González, S. Acevedo, and J. Peláez-Restrepo, Design and control of a buck- boost charger-discharger for DC-bus regulation in microgrids, Energies, vol. 10, no. 11, 2017. doi: 10.3390/en10111847.

[23] M. Monsalve-Rueda, J. E. Candelo-Becerra, and F. E. Hoyos, Dynamic Behavior of a Sliding-Mode Control Based on a Washout Filter with Constant Impedance and Nonlinear Constant Power Loads, Appl. Sci., vol. 9, no. 21, p. 4548, Oct. 2019. doi: 10.3390/app9214548.

[24] E. Ponce and D. J. Pagano, Sliding Dynamics Bifurcations in the Control of Boost Converters, IFAC Proc. Vol., vol. 44, no. 1, pp. 13293–13298, Jan. 2011. doi: 10.3182/20110828-6-IT-1002.02603.

[25] Khongkhachat, S., Khomfoi, S., A Sliding Mode Control Strategy for a Grid-Supporting and Grid-Forming Power Converter in Autonomous AC Microgrids, (2019) International Review of Electrical Engineering (IREE), 14 (2), pp. 118-132. doi: https://doi.org/10.15866/iree.v14i2.16331.

[26] Ouadi, H., Et-taoussi, M., Bouhlal, A., Nonlinear Control of Multilevel Inverter for Grid Connected Photovoltaic System with Power Quality Improvement, (2017) International Review of Electrical Engineering (IREE), 12 (1), pp. 43-59. doi: https://doi.org/10.15866/iree.v12i1.10685.

[27] Di Noia, L., Del Pizzo, A., Meo, S., Reduced-Order Averaged Model and Non-Linear Control of a Dual Active Bridge DC-DC Converter for Aerospace Applications, (2017) International Review of Aerospace Engineering (IREASE), 10 (5), pp. 259-266. doi: https://doi.org/10.15866/irease.v10i5.13818.

[28] Rached, B., Elharoussi, M., Abdelmounim, E., DSP in the Loop Implementation of Sliding Mode and Super Twisting Sliding Mode Controllers Combined with an Extended Kalman Observer for Wind Energy System Involving a DFIG, (2020) International Journal on Energy Conversion (IRECON), 8 (1), pp. 26-37. doi: https://doi.org/10.15866/irecon.v8i1.18432.

[29] Merabet, L., Chaker, A., Kouzou, A., Boulouiha, H., Elaguab, M., Investigation on the Control of DFIG Used in Power Generation Based on Sliding Mode Control and SV-PWM, (2019) International Journal on Energy Conversion (IRECON), 7 (4), pp. 148-161. doi: https://doi.org/10.15866/irecon.v7i4.17844.

[30] Tesfahunegn, S., Hajizadeh, A., Undeland, T., Ulleberg, O., Vie, P., Modelling and Control of Grid-Connected PV/Fuel Cell/Battery Hybrid Power System, (2018) International Journal on Energy Conversion (IRECON), 6 (5), pp. 168-177. doi: https://doi.org/10.15866/irecon.v6i5.16652.

5. SECOND ORDER SLIDING MODE CONTROL APPLIED TO MICROGRIDS: DC & AC BUCK CONVERTERS POWERING CONSTANT POWER LOADS.

Abstract

Microgrids are designed to connect different types of AC and DC loads, which require robust power controllers to achieve an efficient power transfer. However, the effects of both AC and DC disturbances in the same type of controller make achieving stability a design challenge. Furthermore, in coupled systems where disturbances affect both upstream and downstream in the microgrid. This paper presents an analysis of a second-order sliding-mode control (SOSMC) applied to a microgrid with direct current (DC) and alternating current (AC) power converters. The aim is to simulate the second-order sliding-mode control with buck converters that feed constant DC-DC and DC-AC power loads. The controller was tested considering a unique sliding surface facing external disturbances, such as variations in the frequency of AC converters, sudden changes in upstream voltages, and Constant Power Loads (CPL). The influence of the gain values (K) on the controller was also analyzed. The results show that the controller is robust regarding sensitivity to external disturbances and steady-state error. However, the importance of constant "K" in the model states that exists K-limits values where if "K" is too low a slowdown is presented and the response against disturbances can be critical, and if is too high, an overshoot is presented in the output voltage.

Keywords: *Sliding-Mode Control; microgrid; Buck Converter; Constant Power Load; Power Converter.*

5.1 Introduction

A microgrid (MG) is continuously subject to disturbances and uncertainties due to natural variability in power supplies and loads. MGs require robust controls, and second-order sliding mode control (SOSMC) has been demonstrated to be robust in a wide range of applications: photovoltaic energy conversion [1], medical, aerospace, power converters [2 – 4], and others [5]. It is crucial to continue with the study as the environmental and energy challenges of society suggest that they contribute to the

sustainability and reliability of electrical networks. Consequently, investigating how to improve the performance of MGs by designing a SOSMC is a very practical challenge.

SOSMC retains the advantages of conventional sliding mode control (SMC), such as reduced order dynamics, robustness, and stability. However, the main control objective in the multiple stages of an MG is to maintain the stability of the system. Especially if the MGs have different types of loads, i.e., direct current (DC) and alternating current (AC), and different types of power sources (renewables and storage systems), sharing a common DC bus. Then, the design and implementation of a SOSMC are required to address chattering effects and increase reliability in an MG.

Robust control systems designed for MGs have implemented higher-order SMC to alleviate chattering, which is one of the most significant drawbacks of conventional SMC. Since a power converter is an essential element within an MG, these elements must be designed for multiple types of loads (i.e., DC/DC, DC/AC) to satisfy all the power requirements of applications in the industry and residential grids. Therefore, the control of MGs with different loads must be able to deal with uncertainties and disturbances. The complexity of these systems, as they have so many diverse behaviors in their elements, requires sufficiently robust control so that the loads are not affected by these disturbances. Moreover, stability is crucial if there is a cascade of power converters feeding constant power loads (CPL).

The authors in [4] proposed a suboptimal second-order controller that can work in grid-connected and island-connected operation modes, and the results are compared with traditional PI control. The authors of [6] designed a super-twisted algorithm for DC-DC power converters. In [7], the author proposed two main criteria based on Lyapunov linearization and mixed potential theory to analyze the stability of the cascade system that feeds CPLs. In this research, our objective is to explore all previous concepts acting simultaneously: the use of a higher-order sliding mode control with various power converters (DC-DC & DC-AC) and analyzing the stability of the system from a practical perspective.

However, although these controllers offer novel solutions in terms of sliding control types, in none of these applications, a single control design is tested simultaneously with different real-time applications. In this sense, the present investigation seeks to test the robustness of the control design against disturbances in various types of microgrid applications simultaneously, using a single set of second-order slider controller design parameters.

SMC is not a recent control technique that offers robustness, it is a particular case of what was initially called variable structure systems [8]. Several second-order controllers have been individually documented with Buck converters [2, 3, 9,10]. In addition, [4, 11] tested a suboptimal SOSMC, or with some variations, such as adaptive sliding control [12, 13]. However, the actual performance of a SOSMC in an MG with multiple inverters for different types of loads in AC and DC currents has not yet been tested. Thus, a very common MG must contain several stages in which different currents can feed other loads. However, more research is needed on multistage controls with different types of MG converters with AC and DC circuits testing a unique controller for all stages.

Therefore, this paper presents the design and implementation of a SOSMC in a hybrid (DC & AC loads) MG. The system is proposed to examine the stability of an MG under certain typical disturbances (variations in loads, instability in sources, and alterations in voltage buses). Then, the MG considers CPLs to observe stability against disturbances. First, a microgrid model was implemented in MATLAB Simulink to emulate a real circuit with different sources and loads. In addition, the contributions in this paper are as follows:

1. SOSMC offers a fast and stable response to disturbances for AC and DC buses.
2. A single SOSMC can provide robustness to a microgrid that experiences disturbances in 3 stages (Main Bus, A.C. and D.C. Buses), given that the appropriate manifold and parameters are selected.

3. The selection of the constant value in the SOSMC manifold is of utmost importance, as an improper choice of this value may lead to chattering and/or overshot phenomena in the output signal.

The paper contains three more sections. Section 2 presents the materials and methods used in this research, with mathematical fundamentals and simulations. Section 3 presents the results, analysis, and discussions obtained from the experiments. Finally, Section 4 considers the conclusions.

5.2 Material and Methods.

5.2.1 General methodology

The methodology used a dynamic model representing a circuit as an object of study attached to a microgrid. The model was created in Simulink using the SimScape library to emulate real applications and disturbances.

Previous studies indicate that the control is robust in a microgrid if other strategies, such as adaptive control are used simultaneously: In [12], the paper presents an adaptive suboptimal second-order controller that can work in grid-connected and island operation modes, and the results are compared with traditional PI control. In [6], the paper presents a super-twisted algorithm for DC-DC power converters. In [7], the author proposes two main criteria based on Lyapunov linearization and a mixed potential theory to analyze the stability of cascade system feeding CPLs, similarly in [14]. In other applications such as robotics, this type of adaptive sliding control is also used as in [15] [16]. Another technique such as fuzzy logic controller based on sliding mode control is also proposed in [17]. In this research, we aim to explore some previous concepts acting simultaneously: using a higher-order sliding mode control with diverse power converters (DC-DC & DC-AC) and analyzing the system stability from a practical perspective. The implemented system is a three-stage microgrid. The first stage is a main bus with the control

objective of maintaining stability in the DC bus against possible disturbances. The second stage is a circuit with a DC/AC controller aiming to guarantee waveform and frequency stability in the face of sudden changes upstream and in the loads. The final stage is a circuit with its controller for DC loads. All controllers consider a second-order sliding mode control and share a single parameter layout. In this sense, it is considered a system with a single design has not been previously tested in the current literature.

5.2.2 Architecture

The microgrid is a small and smart power system with power sources, AC buses, DC buses, power controllers, and loads. Figure 5.1 shows the DC-AC microgrid implemented that includes the basic elements to supply the power demand.

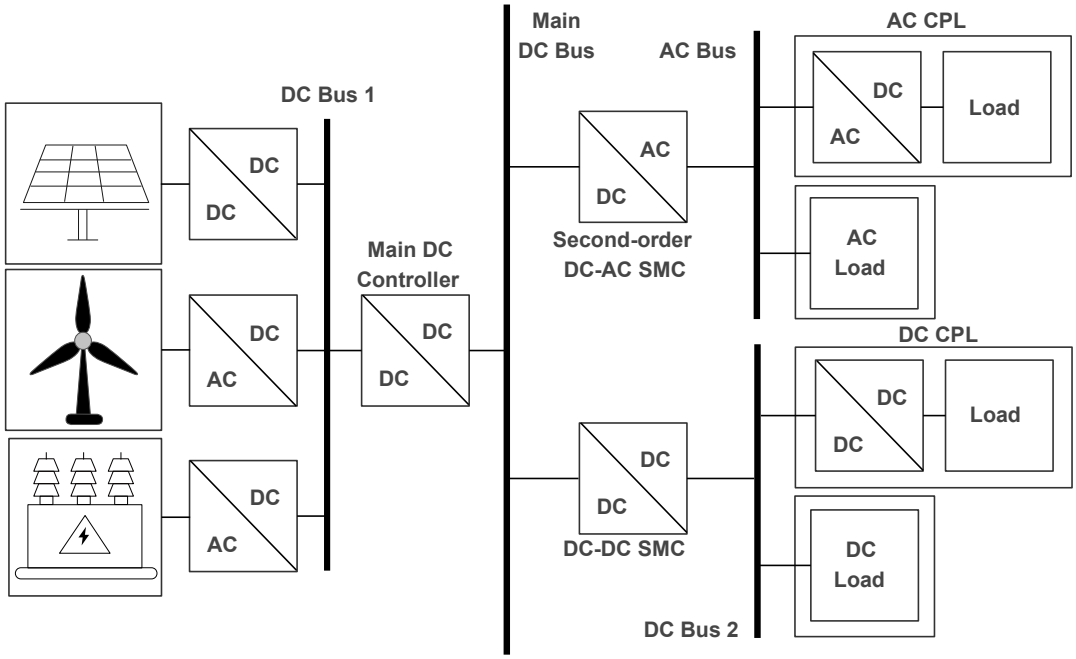

Figure 5.1. *Diagram of the AC-DC microgrid.*

On the left side of Figure 5.1, the microgrid considers renewable energies such as photovoltaic and wind generators, and an AC power grid is also connected. All these

sources have power converters to transfer power from DC or AC circuits to the DC Bus 1. Then, in the first Main DC controller, an SOSMC is implemented to control the Main DC Bus, which regulates the voltage at this point. After the main DC controller, two additional controllers are dedicated to keeping the voltage stable in the loads. The second controller is a DC-DC SOSMC that regulates the voltage to a DC CPL load. The third controller is a DC-AC SOSMC that regulates the voltage on the AC Bus where an AC CPL is connected. These three controllers mentioned previously are the object of analysis mainly. For the Main DC Controller and DC-DC SMC, the circuit uses DC-DC buck converters with the following parameters defined in Table 5.1.

Item	Element	Value
1	Load Resistor	10 Ω
2	Inductance	2.47 mH
3	Capacitor	46 μF
4	Source	320 V
5	Vreference	120 VRMS
6	Frequency	60 Hz
7	Disturbance Resistor	2 Ω

Table 5.1. *Parameters for the DC-DC buck converter.*

5.2.3 Power controller

Figure 5.2 presents the microgrid implemented in MATLAB-Simulink software. The Main DC Bus voltage is obtained by controlling a DC-DC Buck converter. The DC Bus 2 voltage is the result of the response of the second controller, aiming at a set point established as required by the application. For the AC Bus, a third SOSMC controller was implemented; the full-bridge inverter is a typical inverter that requires four switches simultaneously, as presented in Figure 5.2, which are controlled by *u3* and $\bar{u}3$ control signals. Finally, the AC CPL and the DC CPL were also designed using Buck converters controlled by SOSMC. In this model, the switch used was the MOSFET. The design of the parameters for the previous Buck converters was calculated

depending on the typical operational conditions of each stage. The red and blue colors in figure 5.2 refer to direct current voltage polarities.

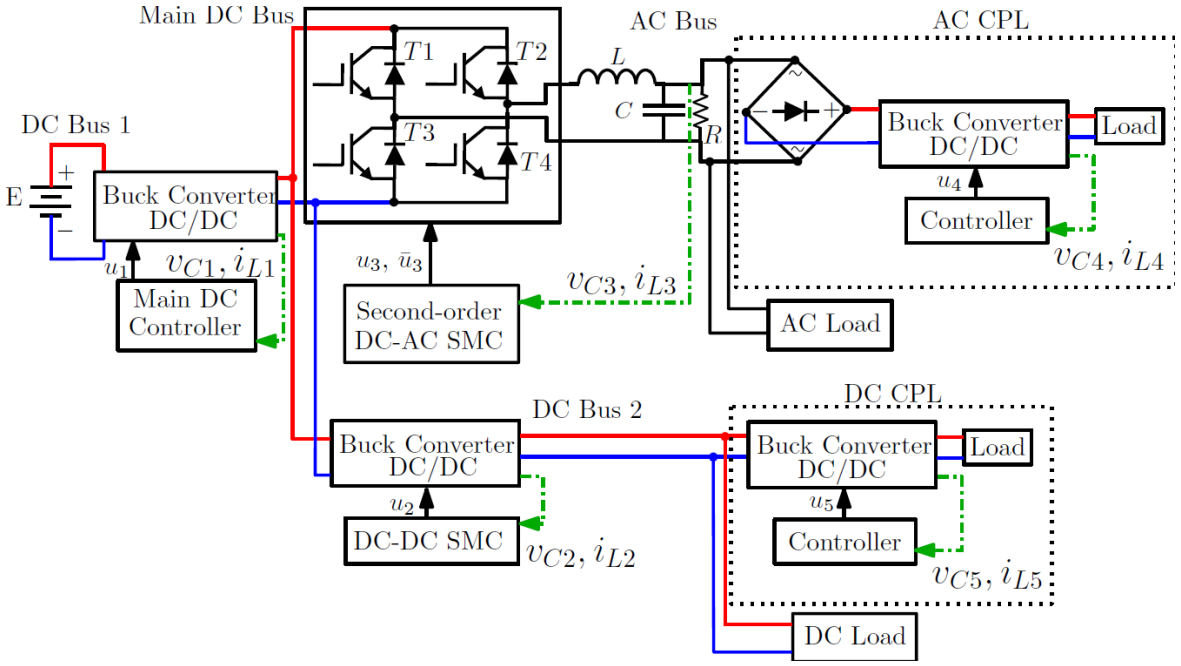

Figure 5.2. Diagram of the AC- DC Microgrid

5.2.4 Mathematical model of the controller

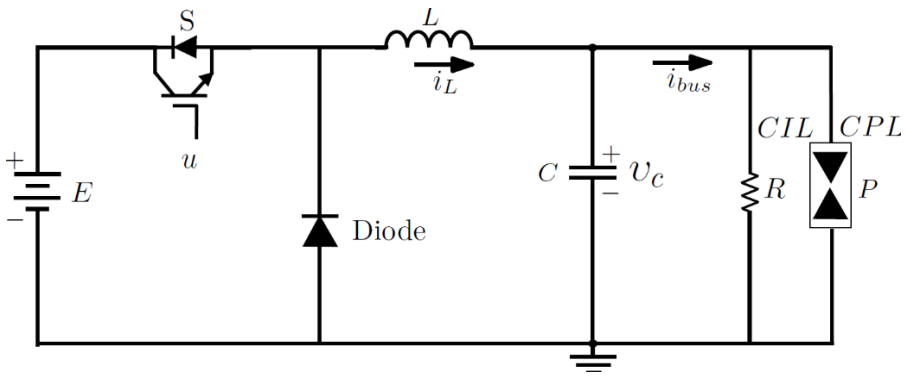

Figure 5.3. *Circuit model of the Buck connected to the CIL (R) and CPL (P).*

The total current supplied by the electrical circuit is equal to the sum of the current in the CIL and the current in the CPL as shown in equation (5.1):

$$i_{bus} = \frac{V_c}{R} + \frac{P}{V_c} \quad (5.1)$$

where i_{bus} is the current supplied by the circuit, R is the constant resistance of the CIL, P is the active power of the CPL, and V_c is the voltage of the capacitor. The equivalent resistance of the circuit can be obtained according to the voltage and the current in the bus as expressed in Equation (5.2):

$$R_{eq} = \frac{V_c}{i_{bus}} \quad (5.2)$$

5.2.5 Dynamics of buck converter (PC SMC)

The mathematical models used to represent the dynamics of a buck converter that feeds the CIL and the CPL are presented in Equations (5.3) and (5.4):

$$L\frac{d_{iL}}{dt} = uE - V_c \quad (5.3)$$

$$C\frac{d_{Vc}}{d_t} = i_L - \frac{V_c}{R} - \frac{P}{V_c} \quad (5.4)$$

In these equations, the term L is the inductor, C is the capacitor, Vc is the instantaneous voltage of the capacitor and iL is the instantaneous current of the inductor. As defined previously in the model, the term E is the voltage of the power source. The term R represents the constant resistance of the load connected to the bus, P is the active power of the load, and the term u is used to represent the switching function with values {0,1}.

5.2.6 Response of the controller

Robust control systems designed for microgrids have implemented higher-order sliding-mode control to alleviate chattering, one of the most significant drawbacks of conventional sliding control. Since a power converter is an essential element within a microgrid, these elements must be designed for multiple types of loads (i.e., DC/DC and DC/AC) to satisfy all the power requirements of the applications in industrial and residential grids. Therefore, control of microgrids with different loads must be able to deal with uncertainties and disturbances. The complexity of these systems, as they have so many diverse behaviors in their elements, requires sufficiently robust control so that the loads are not affected by these disturbances. In addition, stability is crucial if there is a cascade of power converters that feed the CPLs.

SOSMC keeps the main properties and is a generalization idea of first-order SMC. However, from a geometric standpoint, in SOSMC, the sliding surface is the line after the intersection of the two perpendicular planes $\sigma = 0$ and $\dot{\sigma} = 0$ and the states will approach the equilibrium point through this trajectory, as presented in Figure 5.4.

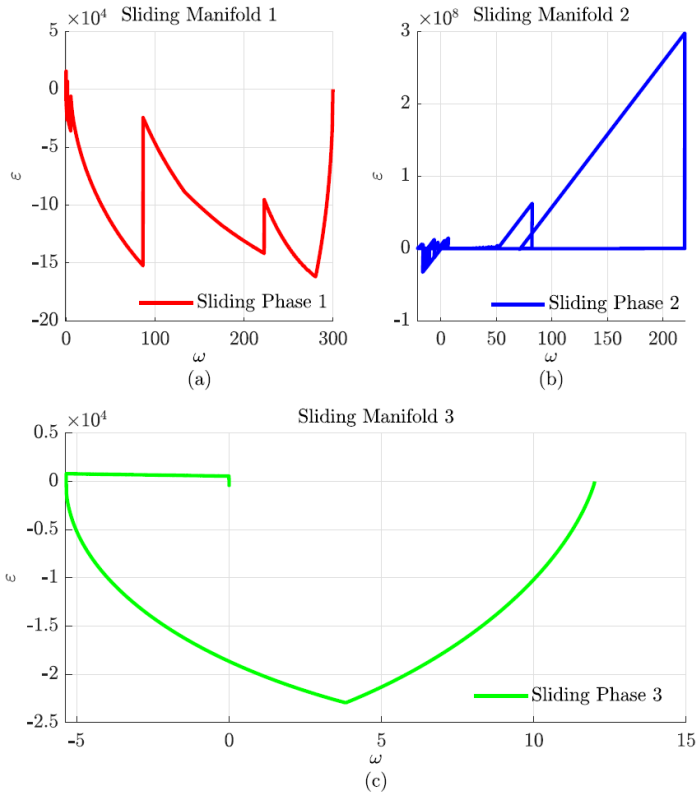

Figure 5.4. *Phase portraits for the three controllers in the MG.*

Figure 5.4 shows the phase portrait for the main controller. This figure shows the phase diagrams for the three controllers. Manifold 1 corresponds to the main DC controller, Manifold 2 to the DC-AC controller, and Manifold 3 to the DC-DC Controller. Those phase diagrams illustrate how a second-order sliding control goes towards the origin in finite time. This is one of the fundamental properties of sliding control.

The control objective states that are required that:

$$\sigma \xrightarrow{yields} 0 \text{ and } \dot{\sigma} \xrightarrow{yields} 0$$

Then, in general we choose the sliding surface as:

$$\sigma = X_2 + cX_1 \qquad (5.5)$$

Were,

$$X_1 = v_{cref} - v_c \qquad (5.6)$$

$$X_2 = i_{ref} - i_L \qquad (5.7)$$

So, if we consider the next sliding variable:

$$\sigma = X_2 + c|X_1|^{1/2}.sign(X_1) \qquad (5.8)$$

Then, the new manifold will be:

$$X_2 + c|X_1|^{1/2}.sign(X_1) = 0 \qquad (5.9)$$

Where X_1 *and* X_2 in a Buck Converter are the error in voltage and current respectively.

In such way, the controller:

$$u = -\rho sign(\sigma) \qquad (5.10)$$

Then, replacing from (5.9) we obtain:

$$u = -\rho sign(X_2 + c|X_1|^{1/2}.sign(X_1)) \qquad (5.11)$$

With

$$\rho >> 0$$

As stated by the author of [18], one of the main particularities in this control is that the SOSMC derivative acts on the sliding variable instead of affecting the first-order derivative. This is performed to push the sliding variable to zero in a finite time and one way to prove that functions with the same characteristics of u maintain stability in more general spaces (i.e., Banach) [19] [20].

5.3 Results.

This section presents the results and analysis of the SOSMC applied to the buck converter and its behavior after disturbances. The results aim to show the effectiveness of the SOSMC in the microgrid. Disturbances considered changes in the voltage reference of the main DC bus, voltage of the DC bus 1, AC frequency from 60 to 120 Hz, and voltage of the CPL.

5.3.1. SOSMC in a DC-AC buck converter

Figure 5.5a shows the response of the buck converter when the reference voltage is set up to 300 Vdc. In this case, the voltage of the DC 1 bus is 400 *Vdc*. Figure 5.5b presents a zoom of the initial response to observe the overshot and settling time. The result indicates that the maximum positive overshoot is 301.75 *Vdc*, corresponding to 0.71 %. The maximum negative overshoot is 299.4 *Vdc*, corresponding to 0.83 %. The settling time for a 2% band is 14 *ms*. After this event, the system reaches the steady-state stability given by the reference value.

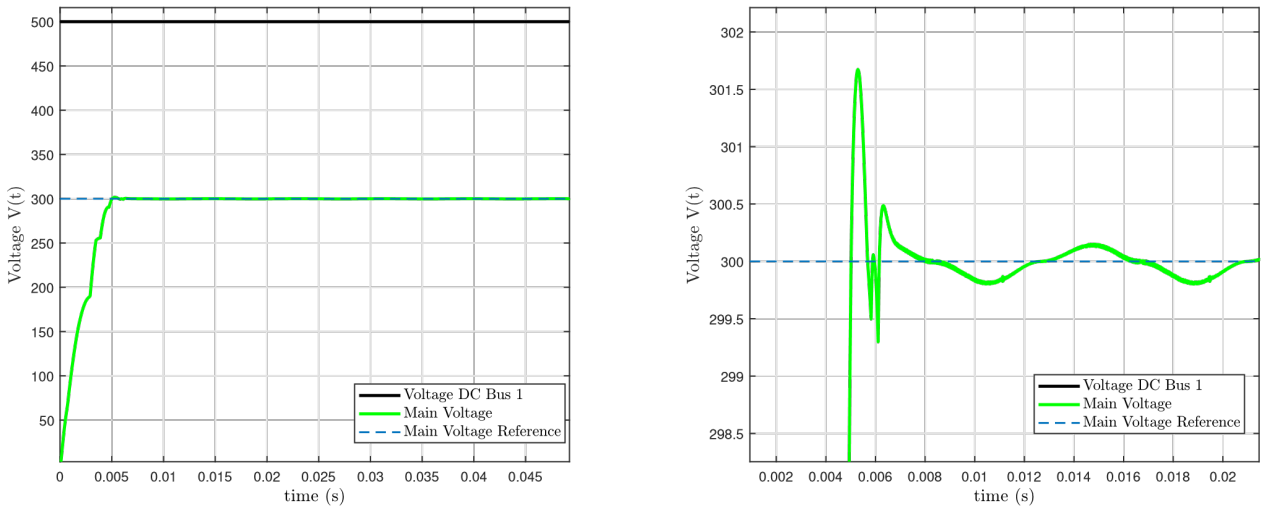

Figure 5.5. *Behavior of the buck converter controlled by SOSMC (a) response to a 300 Vdc step and (b) zoom to see overshoot and settling time.*

5.3.2. Variations in voltage reference of the main DC Bus

Figure 5.6 presents the response of the circuit to a main disturbance in the main DC bus. All plots are graphed in the time domain from 0 to 0.15 s. Figure 5a represents the main DC controller response with changes at the set point. Initially, the reference signal was changed from 0 to 300 Vdc at 0 s. Then a change from 300 to 400 Vdc was made at 20 ms. Subsequently, a change from 400 to 450 Vdc was made at 40 ms. Then a change was made from 450 to 400 Vdc. Finally, a change was made from 300 to 100 Vdc. The results in Figure 5a show that when the first reference is changed to 300 Vdc, an overshoot is presented, and it is greater than the other overshoots. Reference signals less than 155 Vdc are excluded from this rule, which corresponds to the peak value of the AC bus because this bus requires that it be maintained at 110 Vrms, which corresponds to the 155 Vac peak value. Furthermore, as this bus is downstream, the main bus signal cannot be less than this value because the controller cannot maintain the AC bus voltage. It is also observed that the settling time for decreasing references is longer because the buck converter used to keep the main bus controlled uses only one MOSFET. Therefore, the main DC voltage keeps its control value once in the stable region.

Figure 5.6b presents the behavior of the AC voltage in the CPL, which does not present significant variations in the signals after disturbances. Figure 5.6c presents the voltage behavior in the DC-AC CPL for a reference of 48 Vdc, showing that the controller responds quickly to changes and stabilizes the signal. Figure 5.6d shows the voltage in the DC bus when the voltage reference is set to 24 Vdc; it indicates that the voltage stabilizes quickly at the value established for the reference. Figure 5e shows the voltage on the CPL bus for a 12Vdc reference; showing that the signal remains stable after the first change and presenting a first overshoot that is quickly stabilized. Therefore, these last four figures show that with the SOSMC controls, the voltages stabilize after the disturbance. In addition, it can be observed that it regulates the DC signals, and these do not affect the signals of the upstream and downstream buses.

Finally, despite the strong upstream variations, the DC bus and its load (DC voltage in the CPL) remain at their set points.

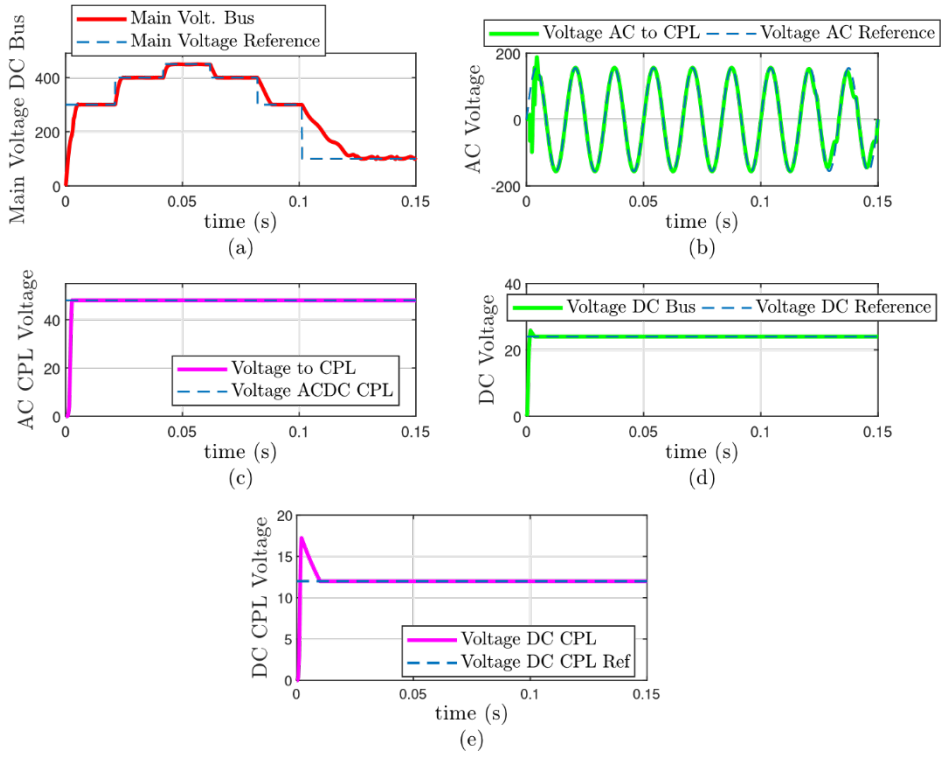

Figure 5.6. *Behavior of voltages after a disturbance in the main DC bus: (a) main DC bus, (b) AC bus, (c) AC CPL, (d) DC bus 2, and (e) DC CPL.*

Table 5.2 shows a summary of the results presented in the previous figures. The first column corresponds to the time in seconds. The second column is the response on the main DC bus. The third column is the response of the AC bus. Finally, the fourth column corresponds to the response in the CPL.

Time (s)	Main DC bus	AC Bus	CPL
0 -0.02	Initial response reaching a set point of 300 Vdc. Settling time: 0.14 ms. Overshoot: 1.33%.	AC signal stable after 7 ms.	AC CPL reaches the reference after 7 ms, and DC CPL reaches the reference after 7 ms.
0.02-0.04	Reaching a set point of 400 Vdc.Settling time: 0.12ms. Overshoot: 5.53%.	AC signal stable	Both CPLs keep stable

0.04-0.06	reaching a set point of 450 Vdc. Settling time: 6ms. Overshoot: 5.53%.	AC signal stable	Both CPLs keep stable
0.06-0.08	Down to a set point of 400 Vdc. Settling time: 6ms. Overshoot: 5.53%.	AC signal stable	Both CPLs keep stable
0.08-0.1	Down to a set point of 300 Vdc. Settling time: 6ms. Overshoot: 5.53%.	AC signal stable	Both CPLs keep stable
0.1-0.14	Down to a set point of 100 Vdc. Settling time: 6ms. Overshoot: 5.53%.	AC signal unstable after 0.12 s	Both CPLs keep stable

Table 5.2. *Time analysis after a disturbance on main DC bus*

Figure 5.7 presents the behavior of the voltage in the main DC bus after a disturbance in the DC bus 1. A change in the voltage of the DC bus 1 is made from 500 Vdc to 400 Vdc at 0.05 seconds. Then a change is made from 400 Vdc to 500 Vdc at 0.1 seconds. It is observed that the voltage on the main DC bus remains stable, and no changes are observed due to disturbances. The behavior of the transient before 20 milliseconds is normal, as shown in the previous analysis.

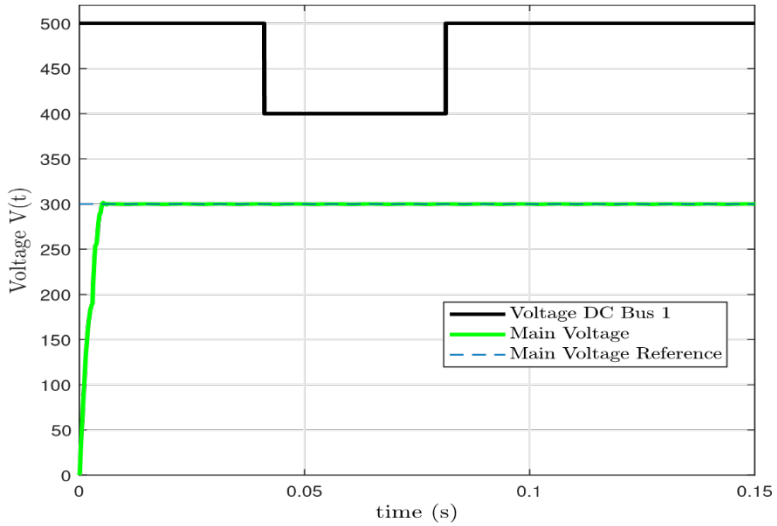

Figure 5.7. *Voltage of the main DC bus after a disturbance in DC Bus 1*

Figure 5.8 presents the error of the SOSMC. Figure 5.8a shows the percentage error on the main DC bus, and Figure 5.8b presents a zoom of the percentage error

from 10 to 50 ms. In the first 10ms, the error is large because of the reference change; however, this result presents normal behavior. After this first time, the results show a small error of 0.065%.

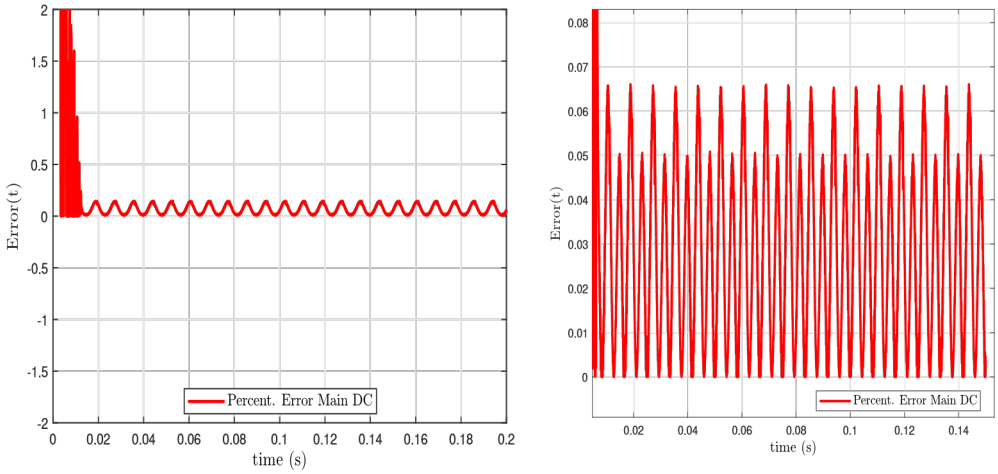

Figure 5.8. *Sliding-mode controller error: (a) percentage error on the main DC Bus and (b) zoom of the percentage error on the main controller.*

Figure 5.9 presents the behavior of the voltage in the main DC bus regarding the variation of the parameter k. Figure 5.9a shows the voltage when the parameter k = 0.5, Figure 5.9b shows the voltage when the parameter k = 3, Figure 5.9c shows the voltage when the parameter k = 10, Figure 5.9d shows the voltage when the parameter k = 15, Figure 5.9e shows the voltage when the parameter k = 20, and Figure 5.9f shows the voltage when the parameter k = 80.

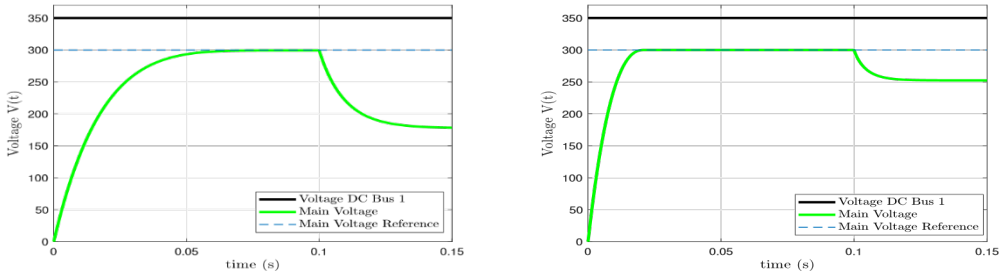

(a) **(b)**

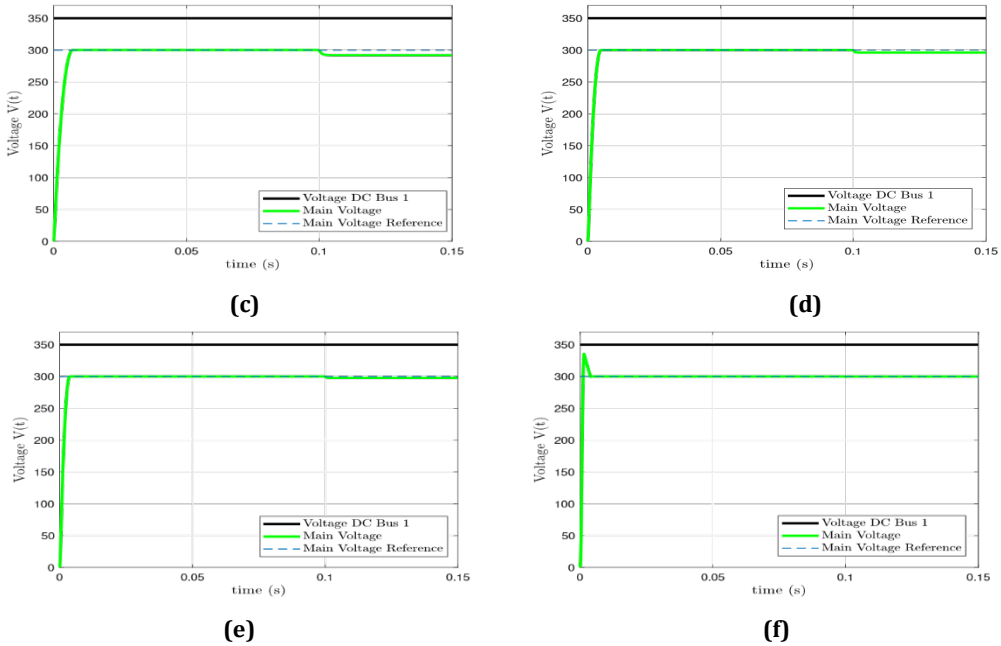

Figure 5.9. *Voltages with respect to variation of parameter k: (a) k = 0.5, (b) k = 3, (c) k = 10, (d) k = 15, (e) k = 20, and (f) k = 80.*

Figure 5.10 presents the controller response after the voltage reference in the main bus was abruptly disturbed from 250 Vdc to 320 Vdc. Furthermore, Figure 5.11a presents the settling time after the change is made from 320 Vdc to 230 Vdc.

The result shows that the output signal follows the reference signals. These results show that the DC bus and CPL voltages are stable despite this intense variation. Furthermore, the results in Figures 5.10 and 5.11 show that the time to reach a new voltage reference is shorter than that required to get a lower voltage reference. This is due to the very nature of the converter, as it only acts on MOSFET devices, and its response to decreasing the voltage depends on internal elements such as capacitors and coils.

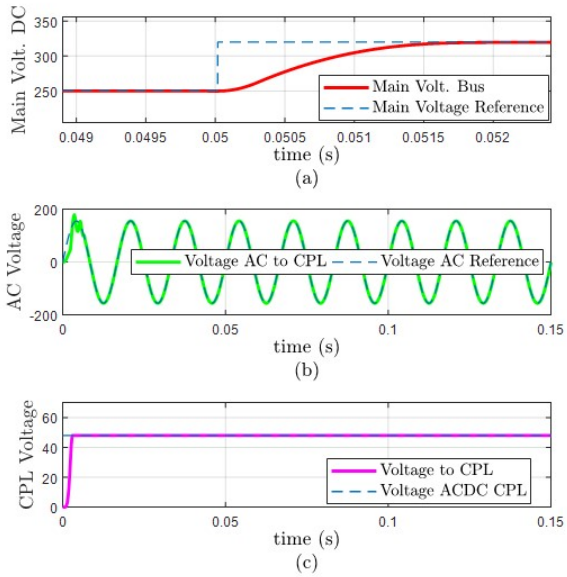

Figure 5.10. *Settling time after an up variation in the set point (a) main voltage, (b) AC voltage, and (c) CPL voltage*

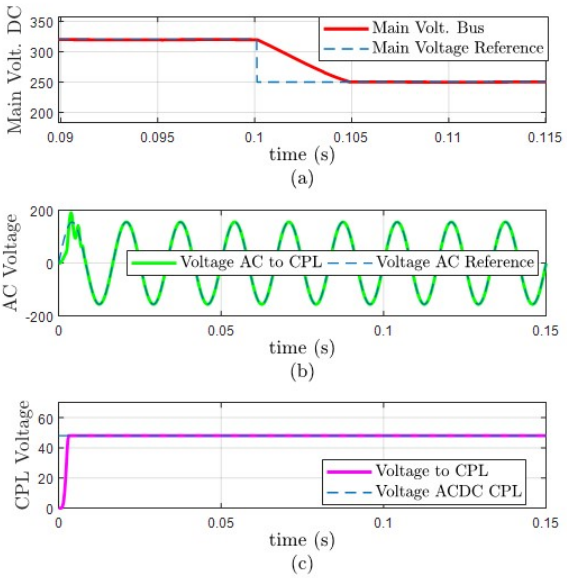

Figure 5.11. *Settling time after a down variation in the set point (a) main voltage, (b) AC voltage, and (c) CPL voltage*

5.3.4. Change in the voltage of DC bus 1.

In a microgrid, commonly, the main voltages fluctuate depending on the sources: i.e., cloud interference on a PV array and wind intermittent on a wind power turbine. Therefore, the following simulations perform some disturbances to evaluate the controller response in the microgrid.

Figure 5.12 presents the behavior of the voltage in the main bus, after a variation in the DC bus from 250 to 320 Vdc (t=0.05s). Then, when t=0.1s a new variation is considered from 320 to 220 Vdc. This figure presents three plots: Figure 5.12a is related to the main voltage bus, Figure 5.12b shows the DC voltage, and Figure 5.12c shows the CPL voltage AC-DC. All plots are graphed in the time domain from 0 to 0.15 seconds. This result establishes that the SOSMC controls keep all the set points stable after a strong disturbance.

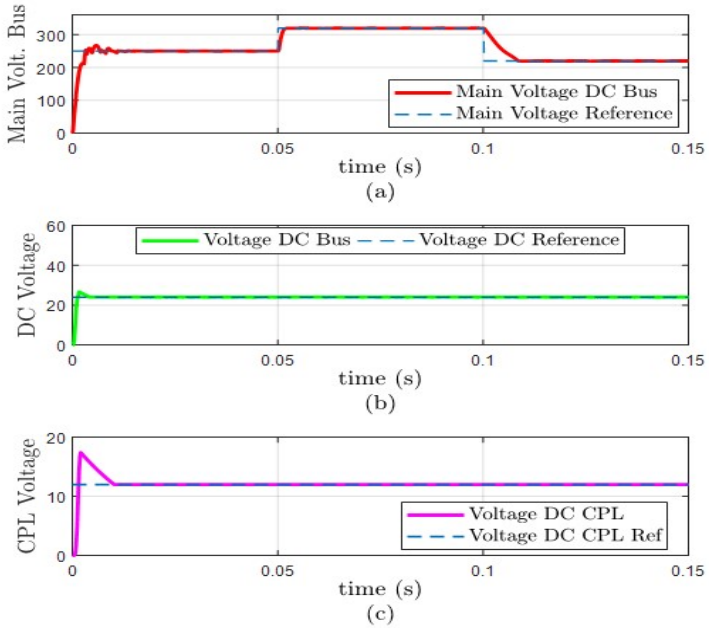

Figure 5.12. *Behavior of voltages when the reference changes in the DC bus: (a) main bus, (b) DC bus, and (c) CPL bus.*

5.3.5. Frequency reference variation in the AC Bus

Figure 5.13 shows the results after a disturbance in the system, given by the change in the frequency of the AC bus. Figure 5.13b presents the variation in the frequency of the AC bus from 60 Hz to 120 Hz (t= 0.05s) VAC and then vice versa (t= 0.1s) simulating a disturbance. This figure presents three plots: Figure 5.13a shows

the voltage diagram related to the main voltage bus, figure 5.13b is the frequency perturbation for the AC bus, Figure 12c shows the voltage of the DC bus, Figure 5.13d shows the voltage of the DC-DC CPL, and Figure 5.13e presents the voltage of the DC-AC CPL. All plots are graphed in the time domain from 0 to 0.15 seconds. This result demonstrates that despite a powerful disturbance in frequency, the branch in DC voltages remains stable.

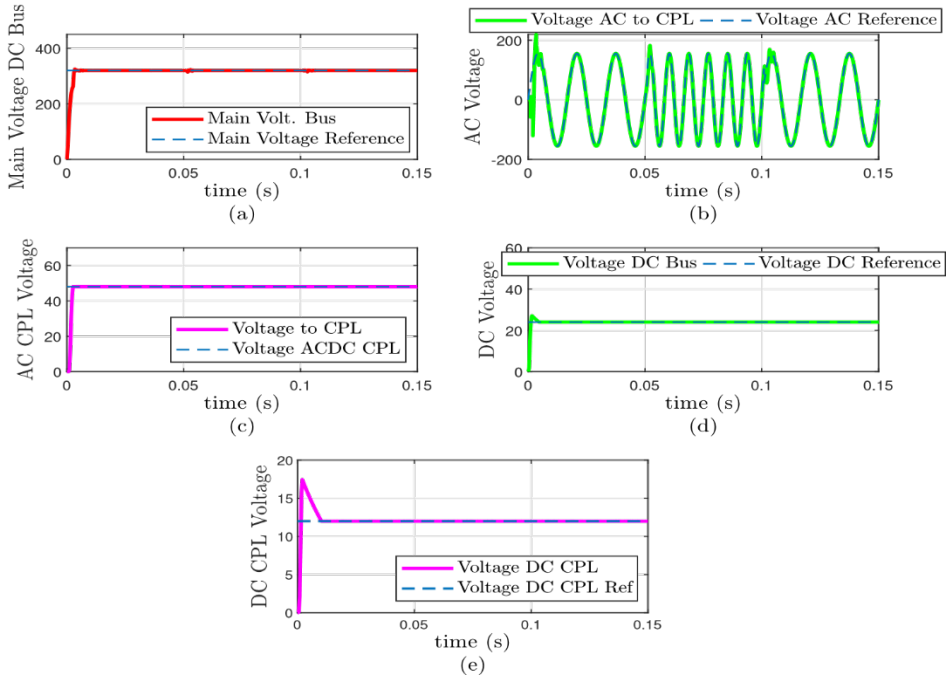

***Figure 5.13**. Behavior of voltages with a frequency change from 60 to 120 Hz. (a) main DC bus (b) AC bus, (c) AC CPL, (d) DC bus 2, and (e) DC CPL.*

Figure 5.14 shows the voltages of the system in the main DC bus, AC bus, and DC bus 2 after a disturbance on the AC CPL. The perturbation was applied in Figure 5.14d. Figure 5.14a indicates that the main DC bus remains stable after the perturbation on the AC CPL. The same behavior is observed for the DC branch with the DC CPL in

Figures 5.14c and 5.14e. All plots are graphed in the time domain from 0 to 0.15 seconds.

This result demonstrates that, despite a strong disturbance in the AC CPL branch, the main DC voltage and the secondary bus remain immovable.

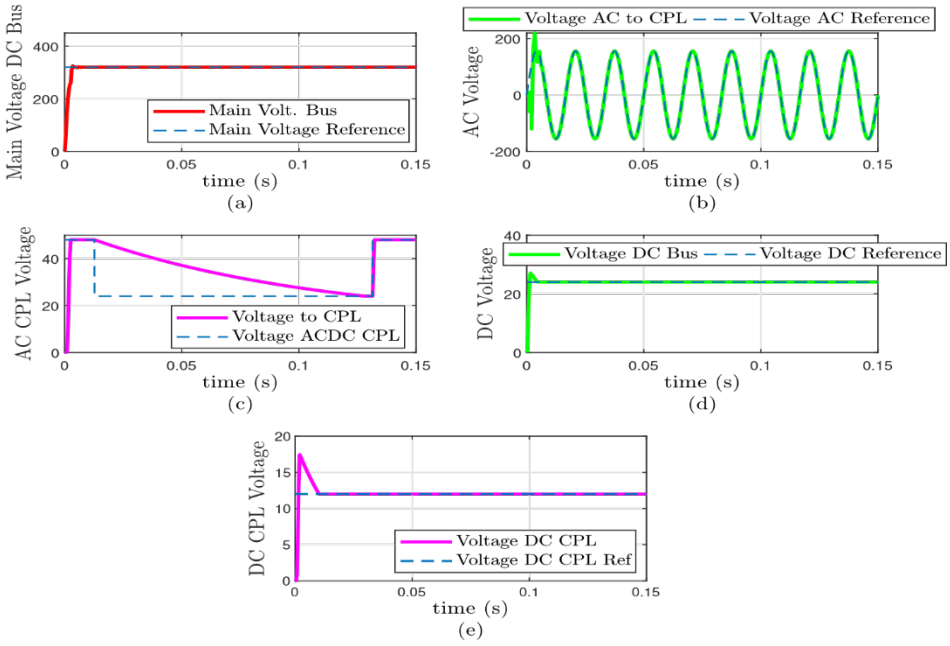

Figure 5.14. *Behavior of the circuit voltages after changes in the set point from 48 to 24 Vdc and from 24 to 48 Vdc. (a) main voltage DC bus (b) Ac voltage, (c) AC CPL voltage, (d) DC voltage, and (e) DC CPL voltage.*

Figures 5.15a and 5.15b show the results after a disturbance in the system caused by a change in the voltage of the AC-DC CPL. Figure 5.15a presents the AC-DC branch after a variation in the AC-DC CPL from 12 Vdc to 18 Vdc (t= 0.05s) and then vice versa (t= 0.1s), simulating a disturbance. This figure presents three plots: Figure 5.15a shows the voltage behavior related to the main voltage bus, Figure 5.15b shows the

voltage behavior of the DC voltage bus, and Figure 5.15c shows the voltage behavior of the DC-DC CPL voltage. All plots are graphed in the time domain from 0 to 0.15 s.

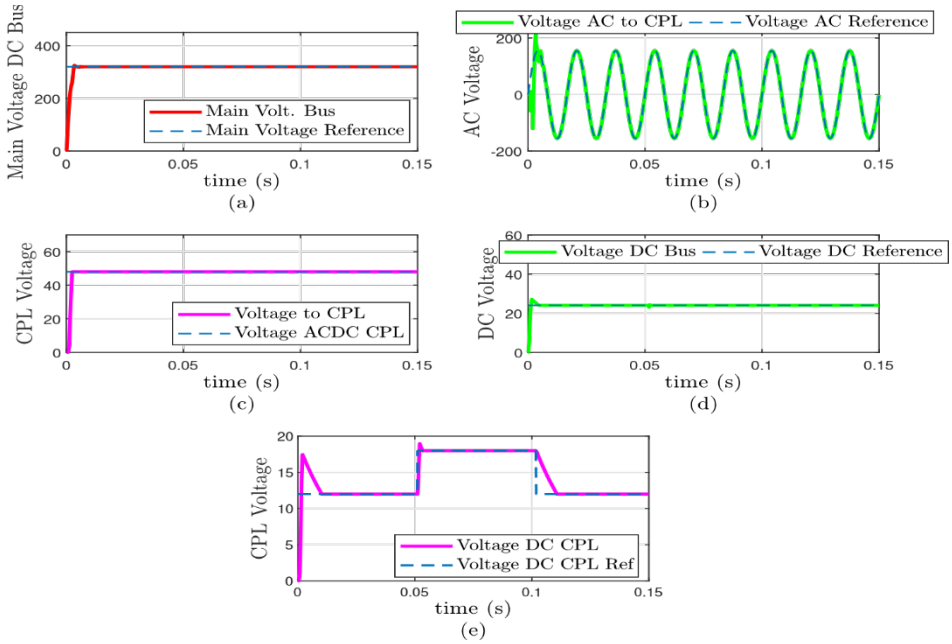

Figure 5.15. *Voltage behavior after a change in voltage reference in the DC-DC CPL from 12 to 18 Vdc and vice versa: (a) main bus, (b) AC bus, (c) CPL bus, (d) DC voltage, and (e) Voltage DC CPL.*

5.4 Conclusions.

This paper presented the design of a SOSMC to operate in a DC-AC microgrid. The results allow us to infer the following conclusions.

- The SOSMC demonstrated robustness in the DC-AC microgrid, with a stable response in terms of voltage and frequency for commercial applications. The average error during the simulations was less than 0.2% for disturbances of 28% in the main voltage feeder.

- Empirically, the constant on the design surface, which must be > 0, represents substantial consequences in the controller response. The correlation showed that a higher k produces a faster response. However, it will be overcome with a higher chattering effect at a determined value. Second, a higher value of 'k' will have a higher capacity to compensate for disturbances.

- The SOSMC demonstrated stable performance against frequency variations: After a substantial variation of 60 Hz (from 60 to 120 Hz) in the input signal set point, the SOSMC maintains stability in all stages of the MG.

- SMC is not a novel control. However, the demonstrations presented in this thesis show evidence that, for modern applications, it is considered to have robust behavior. With a simple mathematical model, applied from a practical standpoint in an application of high relevance and importance, it was shown to provide the required stability for industrial and residential microgrid applications.

- In the case of alternating-current controllers, it was observed that the second-order controller presents excellent stability, even for changes in the frequency of up to 60 Hz concerning its original set point. In DC-DC converters, simple and SOSMC

controllers showed a much higher response speed and less overshoot than conventional PID-type control.

- There are still restrictions from the methodological standpoint, such as the dependence on the speed or sampling frequencies with which different results are obtained depending on the selection of this frequency. It is suggested to continue with the investigation to a completely real model with commercial micro network equipment that allows validation of the findings. In this way, the functionality of the SMC controllers would be empirically demonstrated.

References

1. *Gursoy, M.; Zhuo, G.; Lozowski, A.G.; Wang, X. Photovoltaic Energy Conversion Systems with Sliding Mode Control. Energies 330 2021, 14, 6071.*
2. *Ding, S.; Zheng, W.X.; Sun, J.; Wang, J. Second-Order Sliding-Mode Controller Design and Its Implementation for Buck Converters. IEEE Trans. Ind. Inf. 2018, 14, 1990–2000.*
3. *RakhtAla, S.M.; Yasoubi, M.; HosseinNia, H. Design of second order sliding mode and sliding mode algorithms: a practical insight to DC-DC buck converter. IEEE/CAA J. Autom. Sin. 2017, 4, 483–497.*
4. *Cucuzzella, M.; Incremona, G.P.; Ferrara, A. Design of Robust Higher Order Sliding Mode Control for Microgrids. IEEE Journal on Emerging and Selected Topics in Circuits and Systems 2015, 5, 393–401.*
5. *Le Nhu Ngoc Thanh, H.; Hong, S.K. Quadcopter Robust Adaptive Second Order Sliding Mode Control Based on PID Sliding Surface. IEEE Access 2018, 6, 66850–66860.*
6. *Rakhtala, S.M.; Casavola, A. Real-Time Voltage Control Based on a Cascaded Super Twisting Algorithm Structure for DC–DC Converters. IEEE Trans. Ind. Electron. 2022, 69, 633–641.*
7. *Du, W.; Zhang, J.; Zhang, Y.; Qian, Z. Stability Criterion for Cascaded System With Constant Power Load. IEEE Trans. Power Electron. 2013, 28, 1843–1851.*
8. *Utkin, V. Variable structure systems with sliding modes. IEEE Transactions on Automatic Control 1977, 22, 212–222. https: //doi.org/10.1109/TAC.1977.1101446.*
9. *Songbin, L.; Zhiyuan, F.; Yang, G.; Hai, K.L.; Peng, W. Second-order sliding-mode control of synchronous buck converter based on sub-optimal algorithm. In Proceedings of the 2017 Asian Conference on Energy, Power and Transportation Electrification (ACEPT), 2017, pp. 1–6.*
10. *Kaplan, O.; Bodur, F. Second-order sliding mode controller design of buck converter with constant power load. Int. J. Control 2023, 96, 1210–1226.*
11. *Cucuzzella, M.; Lazzari, R.; Trip, S.; Sandroni, C.; Ferrara, A. Robust voltage regulation of boost converters in DC microgrids. In Proceedings of the 2018 European Control Conference (ECC), 2018, pp. 2350–2355.*
12. *Incremona, G.P.; Cucuzzella, M.; Ferrara, A. Adaptive suboptimal second-order sliding mode control for microgrids. Int. J. Control 2016, 89, 1849–1867.*
13. *Han, Y.; Ma, R.; Cui, J. Adaptive Higher-Order Sliding Mode Control for Islanding and Grid-Connected Operation of a Microgrid. Energies 2018, 11, 1459.*
14. *Wu, J.; Yang, L.; Lu, Z.; Wang, Q. Robust adaptive composite control of DC–DC boost converter with constant power load in DC microgrid. Energy Reports 2023, 9, 855–865. Selected papers from 2022 International Conference on Frontiers of Energy and Environment Engineering, https://doi.org/https://doi.org/10.1016/j.egyr.2023.04.199.*

15. *Yi, S.; Zhai, J. Adaptive second-order fast nonsingular terminal sliding mode control for robotic manipulators. ISA Transactions 2019, 90, 41–51. https://doi.org/https://doi.org/10.1016/j.isatra.2018.12.046.*
16. *Chen, S.Y.; Chiang, H.H.; Liu, T.S.; Chang, C.H. Precision Motion Control of Permanent Magnet Linear Synchronous Motors Using Adaptive Fuzzy Fractional-Order Sliding-Mode Control. IEEE/ASME Transactions on Mechatronics 2019, 24, 741–752. https://doi.org/10.1109/TMECH.2019.2892401.*
17. *Khooban, M.H.; Gheisarnejad, M.; Farsizadeh, H.; Masoudian, A.; Boudjadar, J. A New Intelligent Hybrid Control Approach for DC–DC Converters in Zero-Emission Ferry Ships. IEEE Transactions on Power Electronics 2020, 35, 5832–5841. https: //doi.org/10.1109/TPEL.2019.2951183.*
18. *Shtessel, Y.; Edwards, C.; Fridman, L.; Levant, A. Sliding Mode Control and Observation; Springer New York.*
19. *Levaggi, L. Sliding modes in Banach spaces. Differential and Integral Equations 2002, 15, 167 – 189. https://doi.org/10.57262/die/ 1356060871.*
20. *Triggiani, R. On the stabilizability problem in Banach space. Journal of Mathematical Analysis and Applications 1975, 52, 383–403. https://doi.org/https://doi.org/10.1016/0022-247X(75)90067-0.*

6. FINAL CONCLUSIONS.

The specific conclusions are found at the end of chapters 3, 4 and 5 mainly. However, some of those that are considered main are listed below:

- SMC is not a novel control. However, in the demonstrations presented in this thesis, it shows evidence that for modern applications it is considered to have robust behavior. With a simple mathematical model, applied from a practical point of view, in an application of high relevance and importance, it was shown that it provides the required stability for industrial and residential microgrid applications.
- In the case of alternating current controllers, it was observed that the second-order controller presents great stability, even for changes in frequency of up to 60 Hz with respect to its original set point. In DC-DC converters, both simple and second-order SMC controllers presented a much higher response speed and less overshot than a conventional PID-type control.
- From real circuits the robustness of the system was checked by changing the control parameter k, obtaining a steady-state error of less than 3%. This error was greater than the simulation analysis as expected. Despite the quantization, system discretization, and delay effects present in real systems were modeled, the model continues to show better performance via simulation.

- It was observed by simulation, that the constant on the design surface, which must be > 0, represents substantial consequences in the controller response. The correlation showed that a higher "*k*" produces a faster response. However, it will be overcome with a higher chattering effect at a determined value. Second, a higher value of "*k*" will have a higher capacity to compensate for disturbances.
- There are still restrictions from the methodological point of view, such as the dependence on the speed or sampling frequencies in simulations with which different results are obtained depending on the selection of this frequency. It is suggested to continue with the investigation to a completely real model with commercial electronic equipment that allows validating the findings of this thesis. Thereby, the functionality and robustness of the SMC controllers would be empirically demonstrated.